UNIVERSITAT POLITÈCNICA DE CATALUNYA
BARCELONATECH
Escola d'Enginyeria de Telecomunicació
i Aeroespacial de Castelldefels

TREBALL DE FI DE GRAU

TFG TITLE: Effect of large fuel tanks on aerodynamic performances of blended wing body aircraft

DEGREE: Grau en Enginyeria d'Aeronavegació

AUTHORS: Jose Luis Trillo Arroyo

ADVISOR: Josep Ignasi Rojas Gregorio

DATE: September 7, 2018

Título: Efecto de los tanques de combustible grandes en los rendimientos aerodinámicos de los aviones de fuselaje integradol

Autores: Jose Luis Trillo Arroyo

Director: Josep Ignasi Rojas Gregorio

Fecha: 7 de septiembre de 2018

Resumen

El efecto invernadero es una de las consecuencias más importantes producidas por las emisiones de gases de efecto invernadero (GEI). La industria del transporte es un importante generador de GEI debido a su uso constante de combustibles fósiles como fuente de energía. Por lo tanto, se debe implementar una alternativa al combustible actual para asegurar la supervivencia de las diferentes especies que habitan la tierra.

Esta investigación puede resumirse como la propuesta para el uso del hidrógeno como principal fuente de energía en el sector de la aviación y el estudio de su impacto en el rendimiento aerodinámico y económico. La baja densidad de hidrógeno genera, como consecuencia, la necesidad de utilizar grandes tanques de combustible, los cuáles son difíciles de integrar en los aviones convencionales. El avión de fuselaje integrado ha sido propuesto como la clave de la adecuada integración de los tanques de hidrógeno, debido a su mayor volumen y forma aerodinámica.

Se han estudiado varias integraciones de tanques de combustible para ver su impacto en el comportamiento aerodinámico y económico. Los parámetros a estudiar se han calculado con dos métodos diferentes, los cuales han sido comparados entre ellos. La simulación de CFD nos permite calcular las prestaciones aerodinámicas de la aeronave, tales como las fuerzas y coeficientes de resistencia y sustentación. Además, con información de aeronaves convencionales proveniente de los archivos BADA, se han obtenido varias ecuaciones de regresión, que nos permiten obtener el OEW, el MTOW, la fuerza de resistencia y el consumo de combustible.

Se ha realizado una comparación de la fuerza de resistencia resultante de ambos métodos, concluyendo que los resultados de la ecuación difieren de los de CFD debido a la mayor resistencia inducida de las aeronaves convencionales. Por lo tanto, aunque calcular los parámetros de las ecuaciones de regresión resulta en un peor escenario aerodinámico, se puede considerar como apropiado.

Finalmente se ha realizado un análisis de los diversos parámetros calculados y su respectiva comparación con los de las aeronaves actuales. Aunque el comportamiento aerodinámico y económico puede clasificarse como adecuado, la necesidad de modificaciones en el aeropuerto y las dificultades de implementación de las salidas de emergencia podrían complicar el éxito comercial de modelos similares a los estudiados en este trabajo. Los objetivos del trabajo se han completado con éxito debido a que hemos podido ver el impacto en el rendimiento aerodinámico y económico de un BWB debido a la introducción de grandes tanques de combustible, así como la viabilidad de su uso.

Title : Effect of large fuel tanks on aerodynamic performances of blended wing body aircraft

Authors: Jose Luis Trillo Arroyo

Advisor: Josep Ignasi Rojas Gregorio

Date: September 7, 2018

Overview

The Green House effect is one of the most important consequences of Green House Gases (GHG) emissions. The transport industry is an important GHG emitter due to its constant use of fossil fuels as energy source. Hence an alternative to the current fossil fuels must be implemented in order to assure the the survival of the different species that inhabit the Earth.

This investigation can be summarized as the proposal for the use of hydrogen as the main source of energy in the aviation sector and the study of its impact on aerodynamic and economic performance. The low density of hydrogen generates, as a consequence, the need to use large fuel tanks, which are difficult to integrate in conventional aircrafts.The blended wing body (BWB) aircraft configuration has been proposed as key for the proper integration of hydrogen tanks due to its larger volume and streamlined shape.

Several fuel tank integrations have been studied in order to see their impact on aerodynamic and economic behavior. The studied parameters have been calculated with two different methods, which have been compared. The CFD simulation allow us compute the aircraft aerodynamic performances such as the drag and lift coefficients. Furthermore, with conventional aircraft information from the Base of Aircraft Data (BADA), several regresion equations have been obtained, which give us the OEW, MTOW, drag and fuel consumption as a function of aircraft surface.

A comparison between the drag obtained from both methods has been done, and the conclusion is that the results deduced from BADA differ from those from CFD due to the higher induced drag of conventional aircrafts. Thus, although computing the parameters from the empirical model (regression equations) results in worst aerodynamic performances, the method can be considered accurate enough.

Finally, an analysis of the the several calculated parameters and a comparison with the respective parameters of the current aircrafts has been performed. Although the aerodynamic and economic behavior can be considered as proper, the necessary modifications of airport runways, taxiways, etc., and the difficulties associated with implementation of emergency exits could complicate the commercial success of models similar to those studied in this work. The objectives of the work have been successfully completed because we have been able to see the impact of introducing large fuel tanks on the aerodynamic and economic performance of a BWB, as well as the feasibility of its use.

CONTENTS

LIST OF FIGURES

LIST OF TABLES

LIST OF ABBREVIATIONS

0.1.. Nomenclature and greek symbols

a is the speed of sound
AR is the aspect ratio
b is the wingspan
C is the fuel mass consumption rate of the aircraft.
$\mathbf{C_A}$ is the airport kerosene consumption.
cd is the total drag coefficient.
$\mathbf{c_{d0}}$ is the parasitic drag coefficient.
$\mathbf{cd_i}$ is the induced drag coefficient.
cl is the lift coefficient.
d is the aircraft range.
D is the drag force.
$\mathbf{D_i}$ is the induced drag.
e is the Ostwald factor, and efficiency factor ranging from 0 to 1, which depends on the wing shape (e=1 for wings with elliptical lift distribution).
FoS is the factor of safety to ensure the sufficient fuel for the flight.
g is the acceleration of gravity at MSL.
h is the actual height.
$\mathbf{h_0}$ is the Tropopause base height.
L is the lift force.
l is lift per wingspan unit.
$\mathbf{L_c}$ is the cylinder longitude.
$\mathbf{L_e}$ is the ellipsoid longitude.
m is the hydrogen tank mass.
$\mathbf{N_f}$ is de number of departures in a time interval.
P is the ISA pressure at the current height.
$\mathbf{P_0}$ is the Tropopause base pressure.
Pc is cryogenic pressure.
R is the cylinder radius.
R' is te universal constant for perfect gases particularized for the air.
S is the wing surface.
T is the air temperature at the current height.
$\mathbf{T_0}$ is the Tropopause base temperature.
$\mathbf{T_h}$ is the Thrust.
t is the time per flight.
$\mathbf{t_w}$ is the wall thickness of the hydrogen tank.
TSFC is the constant thrust specific fuel consumption.
$\mathbf{v_c}$ is the TAS.
$\mathbf{V_{cyl}}$: is the volume of the cylindrical hydrogen tank.
$\mathbf{V_{req}}$ is the tank volume required to perform a flight.
W is the aircraft weight.
β is the Lapse Rate
γ is the the adiabatic coefficient.

Γ is the circulation rround the airfoil.
ρ_0 is the Tropopause base density.
ρ_a is the air density at the current height.
ρ_w is the wall material density of the hydrogen tank.
ρ_s is the Synjet density.
σ is the yield strength.

0.2.. Acronyms

AA: Aluminum alloy.
AOA: Angle of attack.
ATC: Air traffic control.
BADA: Base of aircraft data.
BWB: Blended wing body aircraft.
CFRE: Carbon fiber reinforced epoxy.
DOC: Direct operating costs.
GHE: Greenhouse effect.
ISA: International Standard Atmosphere.
JFK: International John F. Kennedy (New York) airport.
LEBL: International Barcelona/El Prat airport.
LEMD: International Adolfo Suárez Madrid-Barajas airport.
LLBG: International Ben Gurión (Israel) airport.
M: Mach number.
MTOW: Maximum Take-Off Weight.
OEW: Operating Empty Weight
Synjet: Synthetic jet fuel (kerosene)
TAS: True airspeed.

INTRODUCTION

The continous growth of the air traffic causes a growth of the fuel consumption. This, in addition to the oil peack, results in future constraints and challenges in the aeronautical sector. Fossil fuels are finite, not renewable, and have a high negative impact on the environment, but in spite of this they are used because of their profitability. Therefore, an alternative to kerosene must be found as soon as possible. A large variety of alternatives to oil have been studied, but the most popular and feasible to implement are hydrogen as a fuel or electrical engines, both with several restrictions, advantages and disadvantages.

Electrical propulsion is based on bateries, which are very heavy. The limitation of the MTOW in addition to the significant weight of the bateries dificults their implementation. The single way to make electical propulsed aircrafts feasible is by means of a breakthrough in batteries, reducing their weight while keeping their energy storage capacity (reducing the weight to energy ratio).

The low density of hydrogen complicates significantly its use as fuel because a suitable storage method must be found that is not detrimental to the aircraft aerodynamics. Hydrogen has been chosen as the source of energy in this project, imposing a multidisciplinary study based on a large number of parameters. The hydrogen volume needed to perform a large distance flight has an important influence on the aircraft consumption and the space allocated for payload (passengers). The actual commercial aircraft, if modified with a large fuel tank, results in a very inefficient geometry in terms of consumption and payload. To improve the economy of the flight and make an attractive project for airlines, the BWB aircraft configuration has been chosen. Several fuel tank implementations have been studied to found the best one in terms of energy to weight ratio.

Most aircraft design processes start with a comparison between the aircraft model to be designed and similar aircraft models currently in use. In this case, supported by the information in the BADA files and with the correct Ansys checking, we can approximate the value of important parameters that define the aircraft performances. The efficiency and requeriments are two of the most important factors to consider which are taken into account in this work. The hydrogen tanks implementation is usually associated with an increase in the volume and the economic efficiency reduction of the aircraft model. Bulky models are already seen in air despite their great expense in fuel, so the need favors that this type of somewhat more inefficient operations are carried out. The first flight of the Beluga XL on July 19, 2018 corroborates what was previously said, given the need to transport large pieces of aircraft. Thus, even though implementing hydrogen has higher costs than kerosene, it would be something that could be assumed, due the environmental benefits of the hydrogen implementation and the lack of oil. Otherwise, the trend of the aeronautical industry is improving the aerodynamic efficiency, so the design should be performed as efficient as possible.

Furthermore, an interior design has been performed in order to estimate the daily economy of several aircraft, approximating the payload in terms of number of passengers.

In brief, the main project purpose is to try to find an efficient way to implement hydrogen as fuel on a medium- or long-range flight, without being detrimental to the airline's economy. To achieve this objective, a deep knowledge of the current and future situations of the several sources of energy for aircraft must be acquired, as well as of the main characteristics, parameters and performances when designing and manufacturing the different aircraft involved in this work. In particular, special attention is devoted to a non-conventional aircraft configuration: the Blended Wing Body (BWB).

CHAPTER 1. FUTURE PROSPECTIVES FOR FUELS IN AVIATION

1.1.. Background

The actual oil consumption rate is unsustainable in terms of quantity and environmental safety.
A huge variety of human activities influence negatively the environment, producing a risk to life on Earth. The fact that burning fossil fuels generates a substantial level of pollution, in addition to the finite oil resources, produces a critical situation in the short-term in the energy system. There are different green and renewable alternatives to fossil fuels, which have already been implemented in many sectors like the automobile industry. Even if these methods can provide the necessary energy, their implementation is not always possible because other parameters like cost-effectiveness must be taken into account.

The aviation sector represents the 2 .5 % of the worldwide energy consumption [1]. In order to maintain the viability of the flights an aviation sustainable fuel must be founded. There are many limitations which complicate the correct implementation:

- Need for a large amount of energy.
- The drag depends directly to the Volume and Geometry so it have a direct impact on the consumption and the viability of the flight.
- The MTOW limits the weight of fuel that can be carried.
- The aviation sector must be economically profitable so the fuel can't be too expensive.

Hydrogen can be used in both liquid and gas state. In order to store a large quantity of fuel, cryogenic LH_2 has been chosen, reducing tank mass and volume. The cryogenic Temperature and Pressure is about 22 $^\circ$ K and $1.45 \cdot 10^5 Pa$ respectively.
Regarding to the acquisition, there are several methods of which the desired one is the cleanest electrolysis, following the fuel requirements mentioned previously. The table 1.1 includes the main methods and its CO_2 emission.

Production Source	**kg** CO_2/khH_2
Steam Methane Reforming	From 10.6 to 19.2
Electrolysis (Average North American electrical generation mix)	From 34 to 42
Electrolysis (Average California electrical generation mix)	From 21.7 to 26.5
Electrolysis (Pulverised coal)	From 60 to 66
Electrolysis (Natural Gas fuelled combined cycle gas turbine)	From 23.3 to 32
Electrolysis (Nuclear)	From 1.5 to 4
Electrolysis (Solar photovoltaic)	From 1.2 to 4.8
Electrolysis (Temperate hydro.)	From 0.9 to 4.4
Electrolysis (Tropical hydro.)	From 0.38 to 128
Electrolysis (Wind)	From 0.55 to 1.24

Table 1.1: Possible hydrogen sources or production routes [2]

The hydrogen source selection depends on several parameters, such as contamination or economy, which are dificult to establish in this work.The hydrogen burning is defined by the chemical reaction:

$$H_2(g) + 1/2 \cdot O_2(g) \rightarrow H_20(g) \qquad \Delta H_f^\circ = -241.8kJ/mol \tag{1.1}$$

The presence of atmosferic air instead of O_2 produces nitrogen oxide in addition to the water vapor, due to its composition with 79.08 % of nitrogen. The exponentially flame temperature and lineraly reaction-zone dwell time of gas turbines influence the quantity of NO released during burning, allowing to minimize the environmental impact. The flammability range of hydrogen is 14 times greater than kerosene, admitting a lower reaction zone temperature. The fast hydrogen burning makes posible a shorten dwell time.

As per the water vapor, it can be a problematic product because of the increased amount released as compared to the Synjet (Table 1.3)and the possibility to induce a radiation imbalance due to the modification of the water content in the troposphere. Above 6000 m, the water vapor has a higher impact on GHE compared to CO_2. On the other hand, the short time of resiliance of H_20 results in an insignifant amount of anthropogenic water vapor in comparison with the atmosphere's natural water content, so maintaining the altitude of cruise flight in the troposphere, the GHE produced by water can be disregarded.
Due to not using fossil fuels, the pollution produced is almost enterily of NO (33% or less of the NO produced by current turbofan engines using combustion chambers with premixing), whitout CO, CO_2, particles, HC, S compounds and odor. [1]

The main challenge is to economically produce large quantities of liquid hydrogen. Whereas the fuel price is increasing, the hydrogen price is expected to decrease, making worthwhile its implementation. As the cost of the travel depends on the fuel price, the awaited variation would affect on the viability of the project. In the aviation industry, the fuel cost for LH represents a 50% of the total DOC[1], so an entire comparison between the actual and expected costs should be performed. The higher hydrogen specific energy reduces the differences of the costs in comparison with the Synjet, making profit by paying up to 2.8 times more than the price of kerosene. Since the price depends on the production route, in some cases the profit increases or decreases. Currently, it is obvious that using green

sources, for the same amount of income, the benefit decreases.

While aviation emissions represent only a small portion of those produced by the total use of fossil fuels, their potential impact on public health and welfare can be significant, especially in areas with a high density of air traffic.

1.2.. Hydrogen

1.2.1.. Properties

Hydrogen has several properties which can enable or complicate its implementation as aviation fuel. The tables 1.2 and 1.3 include the values of the mentioned properties. The general comparisons shown in this section are done respect to the Synjet. The fuel mass carried onboard can be lower to the actual current aircraft due to the higher specific energy of LH_2, so the payload mass can be greater for a given MTOW. In spite of the lower fuel mass, an increase of the fuel tank volume must be considered because of the lower density of LH_2,0.071 kg/l compared to 0.812 kg/l Synjet density. The wider range of flamability and flame speed allows to reduce the environmental impact of both water vapor and NO, as disscused previously. The volume of the engines can also be decreased due to the shorter combustion zone because of the fast hydrogen burning[1].

The low temperature needed to maintain the cryogenic liquid hydrogen requires a highly efficient vacuum insulation. In order to isolate the fuel and preserve the safety, the tank volume will be increased as well as the tank mass.The low toxicity and high volatility increase the aircraft safety in case of spillage or leakage.

Fuel	Boiling Point	Melting point	Boiling Point Density	Combustion Heat
Synjet	From 167 to 266 $^{\circ}C$	-50$^{\circ}C$	0.8 kg/l	42.8 kJ/g
Methane	-161.3 $^{\circ}C$	-182 $^{\circ}C$	0.423 kg/l	50 kJ/g
Hydrogen	-252.7 $^{\circ}C$	-259.2 $^{\circ}C$	0.071 kg/l	120 kJ/g

Table 1.2: General hydrogen characteristics [1]

Fuel	kg CO_2/GJ	kg NO_x/GJ	kg H_20/GJ	Burning velocity (m/s)
Synjet	720	0.4	290	43
Methane	550	0.5	450	40
LH_2	0	0.6	750	265

Table 1.3: Environmental hydrogen characteristics[1]

Finally the implementation of hydrogen as a fuel, maintaining the available Thrust provided by the current Synjet engines, will suppose an increase of the engine life. [3]

1.2.2.. Hydrogen storage

1.2.2.1.. Important parameters in the tank design

The basis of this project is to introduce hydrogen as a fuel in aviation. The hydrogen properties explained before imposes a further study about the fuel storage. Important parameters associated with the fuel storage tanks:

- **Volume**: The tank volume is one of the most important properties in this study because it is the main implementation constrain, and depends on the aircraft performances (e.g., range), as well as the predicted payload.
- **Tank shape**: The tank shape must be studied in-depth due to its relation with volume and geometry, i.e., the aircraft geometry may need to be modified to properly include the tank, being able to assume the implementation efficiency dependance with the shape. The form can be cylindrical, spherical or ellipsoidal. The optimum shape criteria is based on the search of the mimimum stress, enabling a thinner and lighter structure. This criteria position the spherical shape as the optimum, followed by the cylindrical. [4] .
- **Thickness**: The necessary thickness of the skin of the tank depends on the material's yield strength, tank shape and volume. The thickness is several orders of magnitude smaller than the rest of the tank dimensions, so the single influence of this parameter is on the total tank mass.
- **Tank structural mass**: This depends on the material's density, thickness of the skin, and the tank shape and volume.

1.2.2.2.. Design requirements for the tank

The hydrogen properties in addition to the safety required to perform a flight impose several limitations that must be fulfilled. Regarding to the materials, the tanks must made of improved materials with a minimum tensile strength of $1.172x10^8 Pa$. Possible materials are Al-Li alloys (series 8xxx) and CFRE [1,4]. An insulation system must be included in order to reduce the hydrogen boil-off, fulfilling the several requeriments:

- The insulation must allow for aircraft stops of about twelve hours without any fuel loses, and must maintain the pressure in $1.45 \cdot 10^5 Pa$, making necessary an in-depth analysis of the insulation material as well as the venting system and implemented procedure.
- The current on-ground aircraft service times must be kept approximately constant, so it must be possible to refuel the LH_2 tank in a period of time that enables arrival of the aircraft to the gate in 30 minutes. The refueling time depends on several conditions (for example, see the B737-600 in Figure 1.1, where a time of 9 minutes can be observed).

- Control systems and sensors which detect hydrogen must be included as safety measure.

- The hydrogen tank must be sealed off from the atmosphere, preventing the entry of air and immediate freezing. Only helium can be used as a purge gas.
- The hydrogen manufacturing site is limited to the airport proximities due to the hydrogen boil-off and storage time restrictions.
- The operational life of the mentioned systems (insulation,venting, Control systems and sensors) must be the same as the aircraft's operational life.

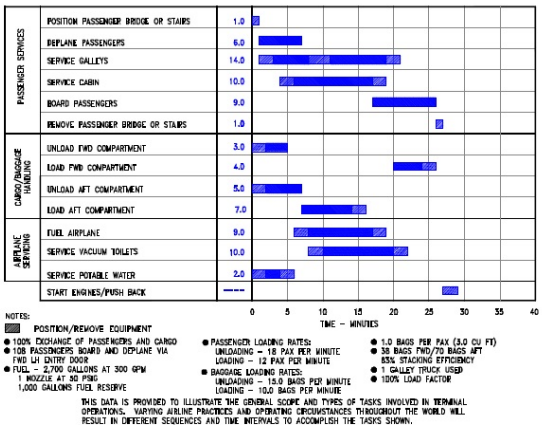

Figure 1.1: Different B737-600 procedure times [5]

1.2.2.3.. Tank Properties formulation

In order to perform a good tank design, the parameters that characterize the tank must be calculated. First of all, the most typical tank design is the one shown in figure 1.2. Its volume V_{cyl} is determined by Eq. 1.2 or Eq., taking into account that the geometry consists basically of a cylinder and two semispheres (or semiellipsoids):

$$V_{cyl} = \frac{4 \cdot \pi \cdot (R)^3}{3} + \pi \cdot L_c \cdot (R)^2 \tag{1.2}$$

$$V_{cyl} = \frac{4 \cdot \pi \cdot L_e \cdot (R)^2}{3} + \pi \cdot L_c \cdot (R)^2 \tag{1.3}$$

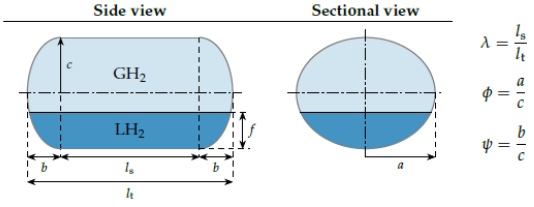

Figure 1.2: Typical cylindrical hydrogen tank

As previously have been comented the required volume V_{req} depends on the aircraft properties and the predicted payload. The relationship can be aproximated as:

$$V_{req} = \frac{4 \cdot C \cdot FoS \cdot d}{\rho_s \cdot v_c} \tag{1.4}$$

The expresion is multiplied by four due to the energy density difference between Synjet and LH_2.The aircraft properties and the predicted payload are defined with C.

The wall thickness t_w of a cylindrical tank can be defined as:

$$t_w = \frac{Pc \cdot R \cdot FoS}{2 \cdot \sigma} \tag{1.5}$$

The tank mass formula is given on Eq 1.6 or Eq 1.7 (two semispheres or semiellipsoids):

$$m = \rho_w \cdot [\frac{4 \cdot \pi \cdot (R + t_w)^3}{3} + \pi \cdot L_c \cdot (R + t_w)^2 - V_{req}] \tag{1.6}$$

$$m = \rho_w \cdot [\frac{4 \cdot \pi \cdot (R + t_w)^2 \cdot (L_e + t_w)}{3} + \pi \cdot L_c \cdot (R + t_w)^2 - V_{req}] \tag{1.7}$$

As the previous formulae for the tank properties are valid only for cylindrical shape, an extrapolation must be performed if an ellipsoidal tank is used. In this case, the skin thickness and tank volume can be adjusted with figure 1.3, while the elliptical tank mass can be adjusted with figure 1.4. Note that the geometrical parameters showed on figures 1.3 and 1.4 can be calculated following the figure 1.2 formulae. The internal overpressure is 1.45 bar ($1.45 \cdot 10^5 Pa$).

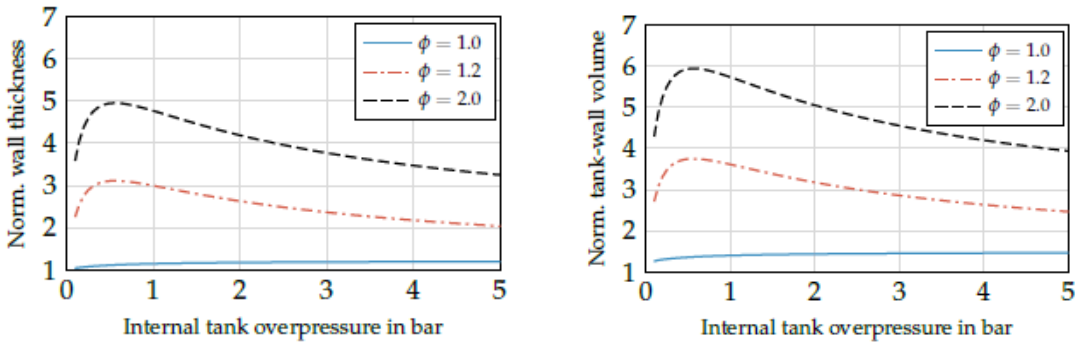

(a) [Thickness comparison between different shell designs

(b) Volume comparison between different shell designs

Figure 1.3: Adjustment Example of Tank Properties [4]

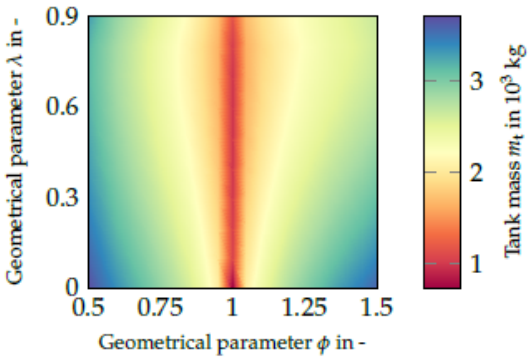

Figure 1.4: Weight dependance with the tank shape [4]

1.2.2.4.. Selection of material for skin and insulation of tank

The typical materials for tank walls used in hydrogen storage and their properties are defined in Table 1.4.

Material	**Density**(kg/m^3)	**yield strength (MPa)**
Steel ASTM-A514	7860	690
Aluminium 2014-T6	2800	410
Titanium Alloy	4460	825
CFRE	1530	1900

Table 1.4: Several tank wall materials[6]

Recently, a NASA project set the AA 2219 as the material with the best accomplishment of hydrogen storage requirements, with $2825kg/m^3$ and a limited stress of 172.4 MPa. AA 2219 has been chosen as the best option for the tank wall in this work.

The insulation materials have also been chosen: Rohacell as a foam as well as MAAMF as sandwich. MAAMF is a multilayer sandwich consisting out of a Mylar layer, followed by two aluminum foil series, another Mylar layer, and a dacron or glass net fabric. Rohacell foam density and thermal conductivity is about $35.24kg/m^3$ and between $5x10^{-3}$ and $3.5x10^{-2}$ W/mK respectively. MAAMF surface density and thickness is about $0.225kg/m^2$ and $1.524x10^{-5}$ m, respectively. Finally, a fairing is added to protect from external damage. The fairing surface density and thickness is about $1.304kg/m^2$ and $1.57x10^{-2}$ m, respectively. The MAAMF and fairing thickness is fixed but the wall and foam thickness depends on the shape and internal pressure of the tank. Taking into account that the wall material density exceeds in two order of magnitude the foam density, although the typical wall thickness is much lower, the total tank mass is principally dominated by the wall parameters.

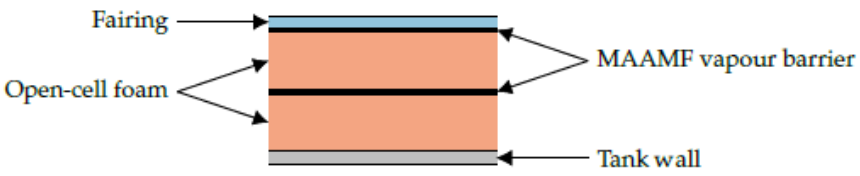

Figure 1.5: Hydrogen tank structure and materials[4]

CHAPTER 2. FUNDAMENTALS OF AERODYNAMICS

The Aerodynamics study must be performed to assure the airworthiness of the resulting aircraft. The supposed situation in order to simplify the problem is a cruise flight.

2.1.. Flight mechanics in cruise phase

The general aerodynamics principles and equations that will be taken into account during this project are explained in this section. First of all, the two components of the aerodynamic force, which strongly depend on the aircraft geometry, are the lift L and the drag D. Both are generated by the flow motion around the vehicle.

The lift is the component of the aerodynamic force perpendicular to the incident flow direction (i.e., the direction of the free stream) and generated by the flow circulation around a body. The wing shape brings on a pressure difference between below and above the wing, being higher under the wing. The pressure difference produces an air flow movement from the lower surface wing root, around the wingtip, towards the upper surface wing root. That flow in addition to a chordwise flow yields a flow speed and direction change. The Newton's third law establishes that the force exerted on the flow by the aircraft is equal to the force exerted on the aircraft by the flow, so if the deviation is toward below, the aircraft it receive a toward up force. This force, in part, opposes to the weight and holds the aircraft in the air. The eq 2.1approximates the Lift force.

$$L = \frac{1}{2} \cdot \rho_a \cdot S \cdot cl \cdot v_c^2 \tag{2.1}$$

C_l depends mainly on the aircraft geometry and AOA, but also slightly on Re and M, and can be calculated with numerical simulations as well as experiments like wind tunnel tests. Reynolds number (Re) is a dimensionless number used in fluid mechanics, reactor design and transport phenomena to characterize the movement of a fluid. Its value indicates whether the flow follows a laminar or turbulent model. Values over 4000 denote a turbulent flow, which is characterized by inertial forces, which tend to produce chaotic eddies, vortices and other flow instabilities. Below 2100 the flow is laminar, which is characterized by smooth, constant fluid motion and viscous forces are dominant. Otherwise, the regime is denominated as transition, a laminar boundary layer will become unstable and turbulent.
The lift can also be defined by assuming Kutta-Joukowski's theorem, which is based on the lift per wingspan unit estimation, i.e. it is a bidimensional scenario due to the assumption of an infinite wing. The lift is defined by the fluid speed around the airfoil, the fluid density and the circulation, being this the line integral of the fluid velocity in a closed curve that contains the airfoil. In other words, the circulation is the amount of fluid arround the airfoil. The lift per wingspan unit can be calculated following the Eq. 2.2

$$l = \rho_a \cdot v_c \cdot \Gamma \tag{2.2}$$

The drag is the component of the the aerodynamic force aligned with the incident flow direction and opposed to the aircraft motion. This component opposes the thrust. The eq

2.3 approximates the drag force.

$$D = \frac{1}{2} \cdot \rho_a \cdot S \cdot cd \cdot v_c^2 \tag{2.3}$$

Like cl, cd depends mainly on the aircraft geometry and AOA, but also on Re and M, and can be calculated with numerical simulations as well as experiments like wind tunnel tests. The drag is composed by different contributions:
The parasitic drag is the resulting resistance due to the movement through a fluid, being composed by the form, skin friction and interference drag:

- The form or pressure drag depends on the shape of the body, increasing with the frontal area, and imposing the need for using streamlined bodies to fly more efficiently (i.e., with lower fuel consumption for a given aircraft mass). It also follows the eq 2.3, so the higher the TAS, the higher the form drag.
- The skin friction drag is the result of the friction between the fluid and the aircraft surface. The aircraft surface in contact with the fluid is named as wet area. The wet area drags some amounts of air divided into layers because of the no-slip condition due to the air viscosity. A resistance to the movement is caused by this amount of air, following the typical friction equation, proportional to the square of the speed. The boundary layer depends on several parameters, being laminar and relatively thin at the front of the object, but turns into turbulent and thicker towards the rear. The alteration of the layer conditions happens in the transition point which depends on the object shape. The laminar layer generates less friction drag, so the shape design should encourage it as much as possible as long as the aircraft would be far from stall, due to the lower resistance to adverse pressure gradient of the laminar boundary layer. Finally, the smaller the wet area, the lower the skin friction drag.
- The interference drag: drag due to the interaction between the boundary layers of different aircraft components.

The lift-induced drag is the drag resulting from redirect of the airflow by the ”lifting body” or wings. The spanwise and chordwise airflow combination produces a speed change, twisting the airflow and generating unstable vortices along the wing trailing edge. The combination of the wing vortices produces the named wingtip vortices, which deflect the airflow behind the trailing edge downwards, and thus inducing downwash behind the wing. The airflow modification reduces the amount of lift generated by the wings, which implies an increase of the angle of attack to maintain the lift force. Hence, there must be a tilt between the lift and the movement direction, dividing the lift into two components, an upward force and an opposed movement force (lift-induced drag). For a given value of lift and wing lay-out, the higher the wing aspect ratio, the lower the induced drag. The lift distribution from tip to tip also affects, being the wing with elliptical lift distribution the most efficient design. It can be obtained using elliptical chord distribution, but it is complicated to manufacture, so other similar lay-outs as tapered wings with straight leading and trailing edges are used. The induced drag can be approximated as eq 2.4 and 2.5.

$$D_i = \frac{2 \cdot L^2}{\rho \cdot \pi \cdot b^2 \cdot e \cdot v_c^2} = \frac{\rho \cdot S^2 \cdot v_c^2 \cdot cl^2}{2\pi \cdot b^2 \cdot e} \tag{2.4}$$

$$c_{di} = \frac{S \cdot cl^2}{2\pi \cdot b^2 \cdot e} = \frac{cl^2}{\pi \cdot AR \cdot e} \tag{2.5}$$

Unlike the rest of drag sources, the higher the TAS, the lower the induced drag in uniform horizontal flight.

The wave drag results from the shock waves produced when the object increases its speed up to the critical Mach number. It is usually included in the form drag. The critical Mach number (Mcr or M*) of an aircraft is the lowest Mach number at which the airflow over some point of the aircraft reaches the speed of the sound. Below Mcr, the airflow around the entire aircraft is subsonic. Above Mcr, the airflow maybe supersonic in one or more regions.

The speed of sound, in addition to the TAS, allows us calculating the dimensionless Mach number, which gives us some indication about the wave drag.

$$M = \frac{v_c}{a} \tag{2.6}$$

The speed of sound depends on the altitude, which can be expressed as eq 2.7

$$a = \sqrt{\frac{\gamma P}{\rho_a}} = \sqrt{\gamma \cdot R' \cdot T} \tag{2.7}$$

The air properties must be defined. As the assumed phase is cruise in horizontal flight, the altitude above the mean sea level (MSL) remains constant at a given flight level (FL).A typical altitude for cruise flight is at the Tropopause, at 11 km of altitude MSL, the atmosphere condition can be approximated with the international standard atmosphere (ISA) formulae of appendix section (appendix A). The altitude is the initial Tropopause layer height so the Temperature, Pressure and Density values are assumed as T_{tropo}, P_{tropo} and ρ_{tropo}.
Summarizing, the total drag coefficient can be approximated as eq 2.8.

$$c_d = c_{d0} + c_{di} \tag{2.8}$$

The parasitic drag coefficient is constant for a given aircraft and the induced drag coefficient depends on lift coefficient. The opposed dependence of the parasitic and induced drag respect to the TAS, in uniform horizontal flight, generates a parabolic tendency of the total drag, as shown in figure 2.1. Generally, some parameter is used to indicate the efficiency, like the lift-to-drag ratio:

$$E = \frac{L}{D} = \frac{Cl}{Cd} \tag{2.9}$$

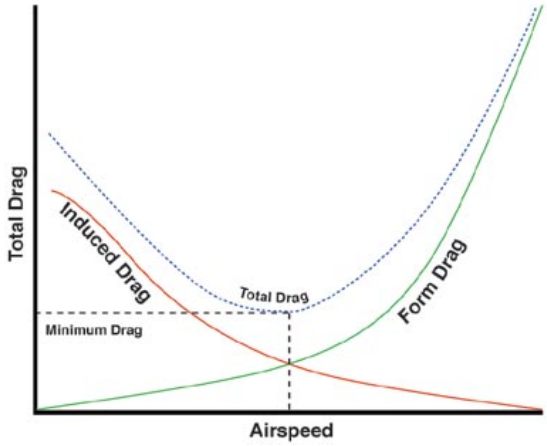

Figure 2.1: Drag type comparison along the speed

The total drag can be modified with an aircraft speed change as can be seen on figure 2.1. Thus, several characteristic speeds can be defined:

- Best endurance speed – the speed that gives the greatest airborne time for fuel consumed.
- Maximum range cruise speed (MRC) – the speed that gives the greatest range for fuel consumed.
- Long range cruise speed - the speed above 3 to 5% of MRC speed providing 99 percent of the absolute maximum specific range.
- Minimum drag speed - the speed that provides the minimum drag.

At a cruise flight, the flight mechanics formulation can be simplified, considering the compensation of the weight by the lift, and the drag by the thrust, keeping a constant altitude and speed.

$$W = L \tag{2.10}$$

$$D = T_h \tag{2.11}$$

Thrust is also involved on the aircraft consumption as shows equation

$$C = T_h \cdot TSFC \tag{2.12}$$

2.2.. Influence of vehicle geometry

The low hydrogen density produces a need for larger tank volume, so the geometry acquires a higher importance and causes more complications because of its implication in the aircraft consumption. The main changes in aircraft performance due to the hydrogen tank implementation are: reduced gross weight (26%), reduced wing with a high voluminous fuselage, a high necessity of area (18%), the smaller engines and cryogenic fuel

system noise reduction, the higher heat sink capacity and finally a Cruise lift-to-drag ratio reduced by 10-18%[1]. These characteristics, if applied to typical commercial aircraft, can result in a higher fuel consumption and lower room for passengers, i.e., an important economic loss.

Finally, the geometry design is strongly affected by tradeoff study about number of passengers and aircraft consumption. There are two possible points of view when introducing the hydrogen tank:
1) a higher volume to introduce more passengers but with a higher consumption,
or 2) the same volume with fewer passengers.

2.2.1.. Baseline aircraft

Several hydrogen tank configurations have been studied by different research teams. In order to understand the implementation possibilities, a search and reading of previous investigations must be carried out. The main investigations are focused on the commercial aircraft geometry modification. Figure 2.2a shows an Airbus design with the hydrogen tanks mounted along the top of fuselage, increasing the aircraft volume and consequently its fuel consumption. Other upper hydrogen tank designs have been done, like integrating four tanks in an A310 [7].

The medium range Airbus aircraft taken into account in this study, the A310, has an MTOW of 150 metric tones, the possibility of carrying up to 243 tourist-class passengers and is powered by two PW-4152 engines of 230000 N static thrust each. The supposed range of the aircraft was selected as 2700 NM. Pohl's investigations set the fuselage-top mounted tank as the most effective configuration in terms of performances, operating costs, handling and safety aspects. For the same range, the fuel spent was about 15.600 kg of LH or 37.000 kg of kerosene for a conventional aircraft.

These data allow as concluding that implementing a huge tank in an aircraft would result in a decrease of the aircraft capacity or in a critical increase of the aircraft fuel consumption. For example, an A310 with tanks mounted along the top of the fuselage would increase its consumption in 15,26%* for a given payload.

*37000 kg with 43600 kJ/kg is equivalent to 13534.7 kg with 119 190 kJ/kg, so the increase can be calculated as: (15600-13534.7)/13534.7)=15.26%.

Figure 2.2b shows the Tupolev TU-155, an experimental aircraft based on hydrogen tank implementation without voluminous cabin but with a reduced capacity of 155 passengers. Pohl has also performed a similar design to Tupolev [7]. The Tupolev aircraft can fly with both cryogenic hydrogen and liquid natural gas. Airbus also has performed a design similar to Tupolev showed on [1].

Figure 2.2c shows an innovative tank integration performed by NASA. The tanks integrated in the wings turn a lifting part of the surface into a blunt body, reducing the produced lift and

increasing the drag in a more drastic way than the upper tank configuration, but without being detrimental to the payload. In a typical commercial aircraft, its implementation can be critical because the lift is only generated by the wings, so an increase in wing surface would have to be introduced probably, to counterbalance the commented reduction in lift.

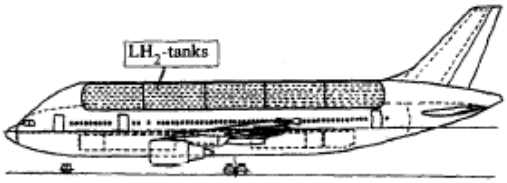

(a)

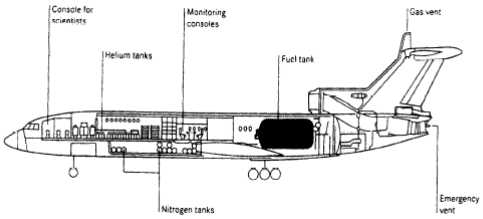

(b)

(c)

Figure 2.2: Hydrogen tank implementations review [1,7,8]

2.2.2.. Blended Wing Body (BWB) aircraft configuration

The expected growth of air traffic demand during the near years, with the current ATC capacity, the performances of the conventional cylindrical fuselage aircraft, as well as the hydrogen tanks implementation, could become problematic and overload the airspace. The actual maximum aircraft capacity is up to 550 passengers in a 3-class layout, reaching the size limit of the conventional designs.
All these factors reduce the viability of a continued extensive use of current conventional cylindrical geometry in a coming aviation scenario.

A list of other configuration alternatives have been studied with the BWB as the most promising concept. Regarding to alternative fuels, the BWB's ellipsoidal geometry could allow an efficient hydrogen tank implementation as well as keeping the current aircraft capacity. Finally, the BWB configuration has been chosen in this work to study the best way of the future aviation, merging two of the most important investigations: the next aircraft and fuel generations.

BWBs are all-wing aircraft without (or almost) non-lifting fuselage, providing fewer friction drag (the usually dominant contribution in streamlined bodies) and higher amount of lift, so a higher efficiency.
This aircraft geometry has a lower wet area to volume ratio, i.e., a BWB with the same wet area than the classical design can allocate a higher number of passengers or larger fuel tanks. The design affects directly on the aircraft consumption as well as its lift-to-drag ratio, so the benefits depend directly on the design efficiency. NASA designs reduce up

to 30% the aircraft consumption in comparison with other aircraft of the same categories. Namely, a lift-to-drag ratio of up to 18.87 has been registered a lift to drag ratio up to 18.87 in a shock free design with $M = 0.8$ [9].

In an investigation by Qin et al. [9], they made a BWB design, and the analysis of the results presented a total drag composed by 77% pressure drag and 23% skin friction drag, fact that must be taken into account in case of modifications, because the modification of a streamlined part of the aircraft can increase critically the total drag. The wingspan is usually about 80 m as a general airport limitation. A higher wingspan would require modifying the airports in order to allow sufficient room for the aircraft on-ground maneuvers. That maximum span limits the aerodynamic performance as well as the number of passengers so other theoretical works study the possibility of implementing a higher or lower wingspan.

About the aircraft stability and control, BWB present a higher number of complications which must be studied. Although these are critical and important issues in aircraft performances, for the sake of simplicity, studying the stability and control is out of the scope of this work.

CHAPTER 3. BWB DESIGN

3.1.. Hydrogen Tank Implementation

The hydrogen tank integration must be designed in order to improve as much as possible the aerodynamic performances. The first modifications on the CAD design have been done taking into account the hydrogen fuel tank volume needed to perform an A380 flight of 15200 km. This assumption can be taken due to the higher wet area of the A380 compared to the BWB. This idea can be carried out with an optimization study of the tank shape and positioning. Once the simulation and parameters have been calculated, an improvement of the designs has been done, resulting in the final designs explained in section 3.2.2.

In this work, the main optimization criterion is the improvement of fuel consumption/economic profit, so a set of hydrogen tank designs have been studied to make an estimation of the flight economy. The first step is to select the tank shape and where to integrate it in the aircraft:

a. We can take advantage of the ellipsoidal shape of the BWB, integrating ellipsoidal tanks. The integration can be done with (BWB_e V1) and without(BWB_e V2) modification of the BWB geometry. As the related previous works anticipated [7], the upper tank integration is more convenient than other choices.

b. A cylindrical tank or various cylindrical tanks can be integrated in a conventional wing position. As not only the wing but the whole BWB aircraft produces lift, the lift to drag ratio is higher than conventional aircrafts. Thus, the slight decrease of this ratio when incorporating non-lifting components (the tanks) should not be very critical. Two different cylindrical tanks implementation have been proposed in this work. First, the BWB_c has the hydrogen tanks in the current commercial aircraft engine positions. The BWB_{ci} design has been performed, reproducing the model of figure 2.2c.

3.2.. Interior Design

In order to compute the maximum payload capacity, a passenger cabin design should be performed. The passenger cabin is the part of the aircraft were the passengers remain during the flight. In this chapter, the passenger cabin design process is explianed.

3.2.1.. Limitations and Specifications

The cabin space is limited by the vehicle space in addition to the structural and geometrical requirements. The security distance between the cabin and outside must be calculated in order to obtain usable space to passengers. The fuselage is composed by Skin, Frame and Stringer. The Frame and the Stringer will be grouped as stiffener.

The skin of the fuselage depends on the section of the aircraft because each zone has its requirements. The skin thickness usually ranges approximately from 1 to 6 mm. The thickness of 6 mm is used only in specific zones, being thus the majority of the skin thickness about 3 mm. The skin and the stiffener thickness will be taken as 0.063 in (1.6 mm) and 1.25 in (31.75 mm) respectively [10], so the total distance between the passenger cabin and the outside is 1.313 in (33.35 mm).

Another important datum is the space allocated for each passenger. Tables 6.7 and 6.8 include the selected distances between two chairsfor each passenger class in a typical 3-class configuration aircraft, reproducing different solutions for A380 and A330 aircraft, respectively. The thickness of the seat is considered to be about 10 cm, and it must be taken into account.

BWB shape complicates the emergency exit implementation. In conventional aircrafts the emergency exit is placed where there is no wing, because these would obstruct the deployment of the slides, but the BWB is an all-wing body, making its typical implementation impossible. Thus, the emergency exit implementation has been not considered.

The minimum height of the passenger cabin has been considered as 165 cm, which is only used in Economy Class. This limitation has been fixed due to the ellipsoidal shape of the aircraft, imposing a decrease of the height in the upper floor of a two floors design.
Finally the aisle distance is about 47 cm, but it will be considered as 50 cm.

3.2.2.. Design Performance

The design process can be performed with a graphic design program; in this case Solid Works. The previous specifications have been considered as possible. The limitations have been introduced in 2D planes. Thus, probably, when translating them into a 3D design, the thickness limitations could have been broken. As the skin thickness may be different depending on the considered part of the aircraft airframe, and an in-depth analysis of this is out of the scope of this work, the approach of 1.6 mm for the whole skin has been considered as proper. Several designs are proposed in this work depending on the available space to introduce the cabin.

3.2.2.1.. One floor

The one-floor cabins have been designed specifically for the ellipsoidal tank aircraft, due to the limitations in space in this aircraft associated with the presence of the tank. It is characterized by a height of 190 cm. The capacity depends on the chosen configuration, so several one-floor cabins have been designed to cover the different flights requirements.

The "BWB_e V1" has a range of 15200 km. The hydrogen tank projects from the aircraft dorsum, so it has a slightly higher consumption respect to the standard kerosene powered BWB. First, using the data in table 6.7, a 3-seats configuration has been implemented, named BWB_e V1.30, which has a capacity of 428 passengers of which 12 are in first

class, 68 in business class and 348 in economy class. A 3-seats and 2-seats configuration, using the data in table 6.8, have also been implemented and named BWB_e V1.31 and BWB_e V1.21 respectively. The 3-seats configuration has a capacity of 448 passengers, of which 12 are in business class, 88 in premium economy class and 348 in economy class. The 2-seats configuration has a capacity of 468 passengers, of which 120 are in premium economy class and 348 in economy class.

The "BWB_e V2" has a reduced range of 11400 km but its shape is identical to the standard kerosene-powered BWB design. We have implemented the same configurations with the same passenger capacities as in BWB_e V1 (V2.30, V2.31 and V2.21), but including another 2-seats configuration, V2.22, with a capacity of 448 passengers, of which 36 are in Business Class and 396 in Economy Class (see dimensions in table 6.8).

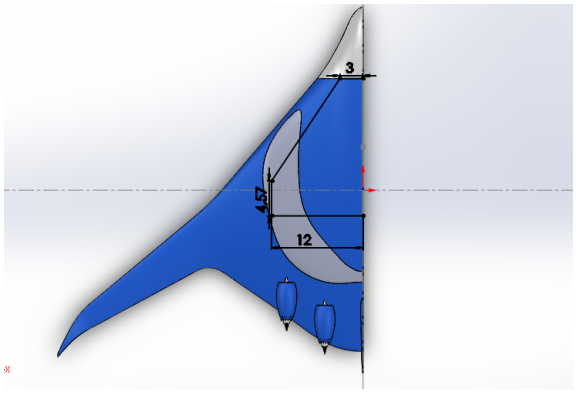

(a) One-floor aircraft layout view

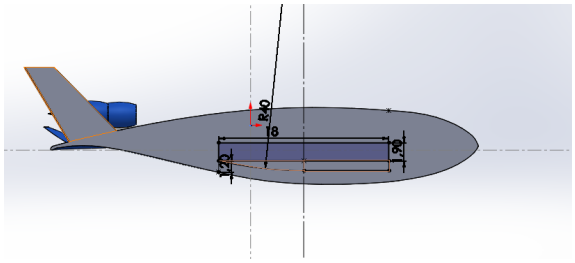

(b) One-floor aircraft lateral view

(c) One floor aircraft passenger cabin design

Figure 3.1: BWB with an ellipsoidal tank V1.3. The zones with a yellow "S" in (c) are are reserved as catering, toilet and dressing rooms. The brown line zones are reserved to store cargo and luggage.

3.2.2.2.. Two floors

The two-floor cabins have been designed specifically for the BWB aircraft with cylindrical tanks, thanks to the large space available inside the aircraft now that the tanks are external. Only a 3-seat configuration has been implemented, with dimensions as shown in table 6.7.
The upper storie is designed with a suitable (smaller) height in order to satisfy the limitations explained in Section 3.2.1. It is characterized by a maximum height of 250 cm, a minimum height of 165 cm and a capacity of 196 passengers which 18 are in first class,

88 in business class and 90 in economy class.
The lower storie is characterized by a height of 2 m and a capacity of 432 economy passengers. The total aircraft capacity is about 628 passengers.

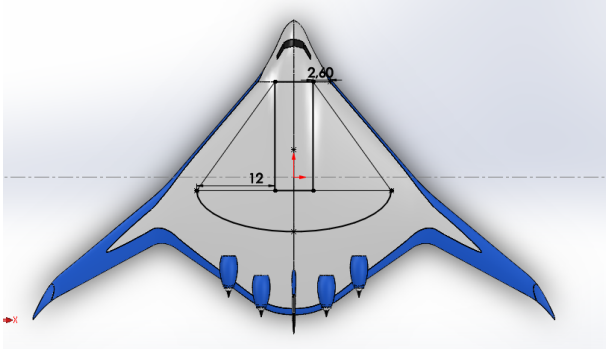

(a) Two-floor aircraft layout view

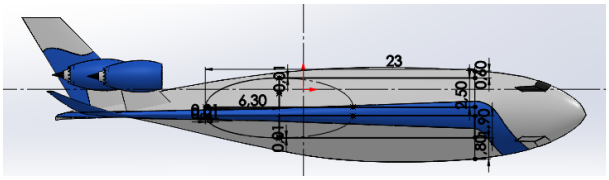

(b) Two-floor aircraft lateral view

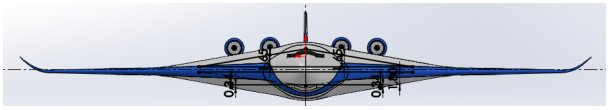

(c) Two-floor aircraft frontal view

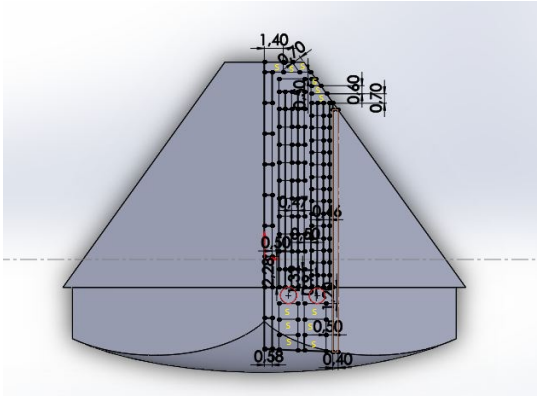

(d) Two-floor aircraft upper passenger cabin design

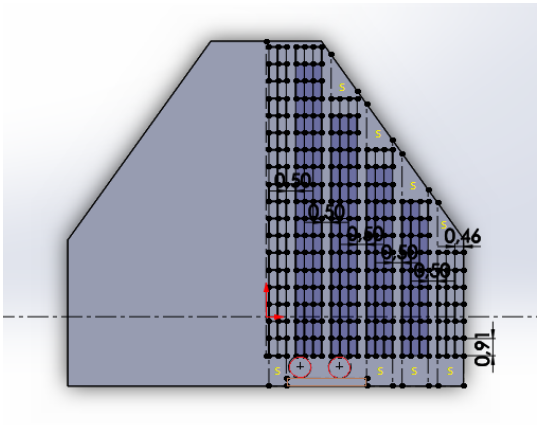

(e) Two-floor aircraft downstairs cabin design

Figure 3.2: BWB with cylindrical tanks. The zones with a yellow ”S” in (d) and (e) are reserved as catering, toilet and dressing rooms. The brown line zones are reserved to store cargo and luggage. The red line zones are stairs.

CHAPTER 4. ESTIMATION OF BWB PROPERTIES AND PERFORMANCE

Once the general characteristics have been chosen, the values of the parameters that characterize the aircraft must be calculated in order to compare them and test if it is feasible and efficient the proposed hydrogen tank BWB aircraft configuration.

4.1.. A simplified aircraft model based on correlation of properties with surfaces

4.1.1.. General explanation

The high complexity and amount of parameters implicated in aircraft design, creates a need for simplifying the problem. Schwarz [11] explains the relationship between MTOW and the rest of the aircraft parameters: ”For the highest level of abstraction, the parameterization of aircraft data is related to only one quantity: the MTOW. Based on a database of existing transport aircraft a functional relationship is established between the relevant aircraft parameters and the MTOW”. Following a similar approach, and since MTOW can be correlated also with aircraft surface, a connection between aircraft surface and other required aircraft parameters has been investigated and used in this work. For example, the larger the aircraft.

First of all, the larger the aircraft wet surface, the larger the skin friction drag. The larger drag entails a higher fuel consumption. Regarding the weight, the relationship between surfaces and masses is noticeable. With the same material, an increase of wet surface implies a heavier aircraft structure, also increasing the OEW.

Finally, the aircraft MTOW is essential to the economic viability analysis. It is an important parameter which depends on several aircraft limitations. One of the most important is the necessity to generate lift to compensate the associated weight. The wing is the main contributor to lift generation, so an increase of the wing surface also implies an increase on the MTOW. A similar conclusion was deduced in Hahn’s research [12].

4.1.2.. Surface acquisition

A CAD acquisition of several BWB and conventional aircraft has been done in order to obtain the required surfaces and perform the pertinent CFD analysis. Solid Works (SDK) is the CAD software chosen in this work. SDK has a measuring tool, located on the ”Calculate” tab, which allows us obtain different parameters from an existing geometry, like the wet and wing surfaces. The several surfaces can be observed in table 6.3.

4.2.. Correlation of aircraft properties with surfaces

When the various important surfaces are known, the involved aircraft parameters as well as their relationship with the surfaces must be studied.

4.2.1.. Base of Aircraft Data (BADA)

BADA is a database that includes a great amount of information on conventional model aircrafts. A code was developed allowing us obtain information from BADA like fuel consumption and aerodynamic performance on cruise flight, OEW and MTOW of the A310, A320, A330, A340 and A380 aircrafts. The Matlab code is shown in Appedix C.

4.2.2.. Obtaining and selecting BWB properties and performance

The developed code calculates also the corresponding BWB parameters using relationships between surfaces and the mentioned variables that were identified in the frame of this research. The drag, consumption and OEW data of the Airbus aircraft, as extracted from BADA and Solidworks, were analyzed.

Data relating to MTOW are also included, for which the source data are from Hahn's article [12]. In each of these cases, en empirical model is proposed, relating the corresponding parameter (i.e., drag, consumption, OEW or MTOW) with the wet or wing surface. The information used to obtain these equations is presented in table 4.1.

Aircraft model	Wet Surface (m^2)	Drag (N)	Consumption (kg/s)	OEW (kg)
A310	1518.70	126021.91	1.67	80000
A320	958.68	47791.46	0.74	43700
A330	2665.58	115009.32	1.70	126000
A340	2822.02	217425.15	2.79	187000
A380	5658.39	302133.35	3.98	282500

Table 4.1: Several parameters of conventional Airbus aircrafts

The procedure to obtain the empirical model is the same for all the parameters. Since several functions could fit well the dependence of each parameter with the wet or wing surface, a selection process must be done to establish the equation providing best fit. Particularly, the two criteria used to choose the most suited equation are the value of the coefficient of determination (R_2, better if closer to 1), and the logical correspondence with the theory of aerodynamics and flight mechanics (i.e., whether one model is more physically sound than the others).

The plotted points and the tested functions can be seen in figure 4.1. The R2 for each function can be observed in table 4.2.

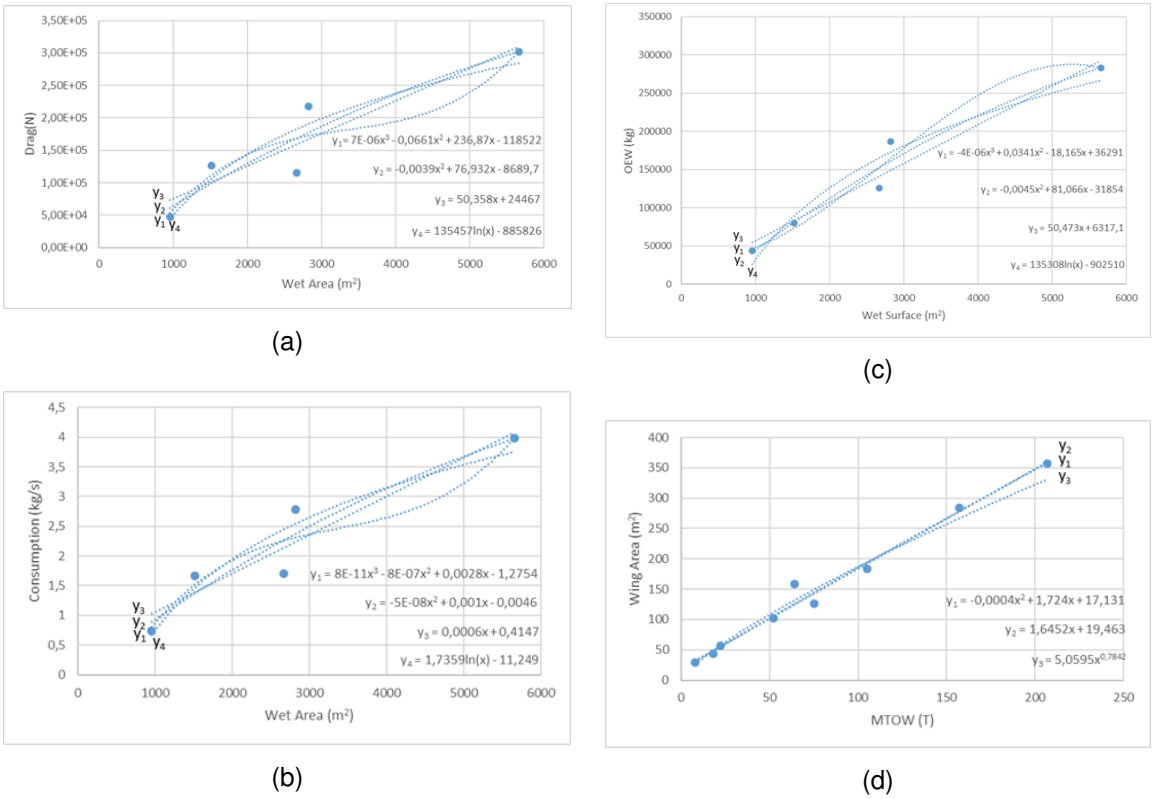

Figure 4.1: Plots showing, as a function of the wet or wing surface, several parameters: (a) drag, (b) consumption, (c) OEW, y (d) MTOW. The tested functions to find the best fit to the data are also shown.

Parameter	function type	R2
Drag	Linear	0.8523
	Polynomial grade 2	0.8626
	Polynomial grade 3	0.7366
	Logarithmic	0.8469
Consumption	Linear	0.8757
	Polynomial grade 2	0.9017
	Polynomial grade 3	0.8400
	Logarithmic	0.8853
OEW	Linear	0.9464
	Polynomial grade 2	0.9615
	Polynomial grade 3	0.9549
	Logarithmic	0.9341
MTOW	Linear	0.9842
	Polynomial grade 2	0.9843
	Exponential	0.9753

Table 4.2: R2 values obtained when fitting various functions to the drag, consumption, OEW and MTOW vs wet surface data.

On the other hand, the selected functions must be physically sound whenever possible. Taking into account the Eq. 2.10 and 2.1, a linear relationship between the aircraft weight

and surface seems reasonable. Hence, the OEW and MTOW could be assumed to have a linear relationship with the wet and/or wing surfaces, respectively.

Following the Eq. 2.4 and 2.1 quadratic relationship between the induced drag and the surface can be considered. Furthermore the Eq. 2.3 with parasitic drag coefficient as a constant, allow us to consider the linear relationship between the parasitic drag and the surface. Even if the parasitic drag is dominant over the induced drag at high cruise speed, taking into account the drag composition (Eq. 2.8), the sum of a linear and quadratic function must be considered, so the drag would be simplify to the quadratic EXCEL function with the wet surface dependence.

Finally, taking into account Eq. 2.12 and 2.11 the linear relationship between drag and aircraft consumption can be considered. Hence, the Consumption could be simplified and assumed to have a quadratic dependence with the wet surface.

Once the functions have been selected, the corresponding parameters must be calculated. The results can be seen in tables 6.1, 6.2 and 6.3

CHAPTER 5. CFD SIMULATION

The CAD files allow us make a CFD simulation that will be used to check the empirical models developed in the previous Chapter and to calculate the aerodynamic performances of the various BWB designs. The CFD simulations will be performed on ANSYS Workbench Fluent.

5.1.. Geometry

The first step is to define the geometry, conformed by the aircraft and the Control Volume in which the simulation will run.

5.1.1.. Aircraft

The body that moves through the fluid is the studied aircraft. The different aircrafts to be compared in this research have been explained in Section 3.2.2. Figure 5.1 shows the different mentioned aircraft configurations. We only need to simulate half of the body thanks to the aircraft symmetry respect to the middle vertical plane, which reduces significantly the simulation time and the necessary system memory. The available CADs for BWB lack Kuchemann carrots, which are a pod positioned on the leading edge or trailing edge of an aircraft's aerodynamic surfaces to reduce wave drag at transonic speeds [13]. As its implementation would result on a wet surface increase, the studied parameters would change, introducing us in a different scenario. In order to check the consequences associated with presence or absence of Kuchemann carrots, its implementation also has been considered.

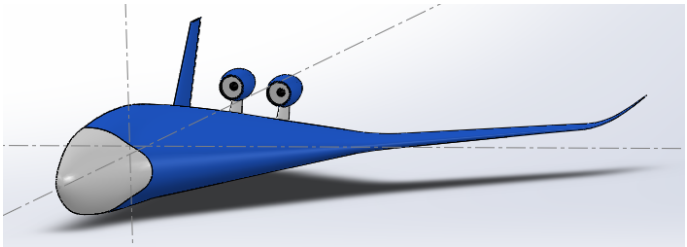

(a) Standard BWB

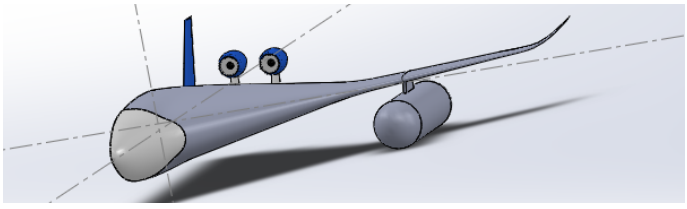

(b) BWB with two cylindrical tanks, First design

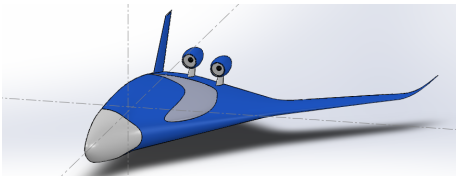

(c) BWB with an ellipsoidal tank

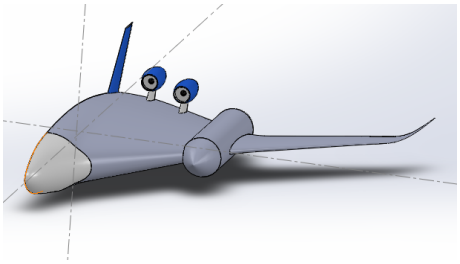

(d) BWB with two cylindrical tanks, Improvement

Figure 5.1: Studied BWB aircraft configurations, where (b), (c) and (d) have a range of 15200 km and (a) a range of 11400km

5.1.2.. Definition of the dimensions of the control volume

The Control Volume must be studied, due to its influence on the results accuracy.
In CAD software, a reference system has been defined, which is composed of 3 axes and the origin. In this work, this point is centered on the aircraft. Regarding the axes, Z corresponds to the drag direction (aligned with the incident flow or free stream), Y corresponds to the lift direction (perpendicular to the previous, also contained in the middle vertical plane), and X is the vectorial product of the others.

About the X and Y direction, the constrains to obtain accurate simulation results of aerodynamic performances are, in relation to lateral dimensions: 1) the BWB wingspan should be less than 80% of the control volume width [14]; and 2) the blocking coefficient (defined as the ratio between the BWB frontal area and the control volume cross-sectional area) should be less than 10% [14].

The upwind and downwind distances (distances from BWB nose to control volume inlet and from BWB tail to control volume outlet) may be more problematic, so longer distances must be taken into account, performing the so-called control volume independence study. This analysis is based on making CFD simulations with increasing size of the control volume until the improvement in results accuracy is marginal, while trying to keep a reasonable computational time. The results shown in table 5.1 lead us to conclude the presence of a negligible change in the three last cases, so to minimize the computational cost, the smallest of these three control volumes has been selected.

downwind distance(m)	upwind distance(m)	cl	cd
20	20	0.122	2.315
80	20	0.223	0.023
100	40	0.222	0.023
120	60	0.223	0.023

Table 5.1: Control volume independence study

5.2.. Mesh

The mesh also affects the accuracy of the obtained simulation results, so the criteria for meshing used during this work must be explained. Explanations will be made about the mesh parameters that will be modified, and other parameters that have an influence on the mesh settings.

5.2.1.. Definition of the boundary conditions and the physics of the problem

CFD analysis requires defining the category and properties of the different fluid and solid zones, as well as the boundary conditions of the studied fluid domain and the physics of

the problem. The selected boundary conditions are inlet, outlet, symmetry plane, body and walls:

- The inlet is an upwind boundary through which the fluid enters into the control volume. Although different parameters can be used to impose how the fluid enters the volume, a typical parameter of the inlet is the speed of the fluid relative to the aircraft, i.e. the TAS. In our case the TAS of simulations is the long range speed of the A380. This case is called “velocity inlet” boundary condition, which is recommended practice to simulate this type of fluid problems. The Inlet is the red plane in figure 5.2a.
- The outlet is a downwind boundary through which the fluid exits the control volume. Although different boundary conditions can be used for the outlet, a typical choice is the “pressure outlet” boundary condition, which is recommended practice to simulate this type of fluid problems. The outlet is the red plane in figure 5.2b.
- The symmetry plane must also be defined in opposition to a simple wall, ensuring that proper results are obtained. The symmetry plane is the red plane in figure 5.2c.
- The walls are those boundaries of the control volume in which the viscous fluid no-slip condition or the ideal fluid tangential speed to the surface is established. The work shown in Section 4.1.2. was performed, in part, to assure enough distance between the body and the walls such that presence of the walls do not affect the results of the simulations. The walls are the red planes in figure 5.2d.
- The body is the solid aircraft embedded in the fluid, the surface of which is in contact with fluid. This Selection is essential to calculate the lift and drag coefficients. The Body is the grey aircraft in figure 5.2.

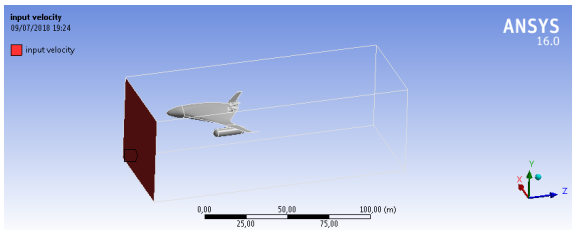

(a) Inlet named as Input velocity

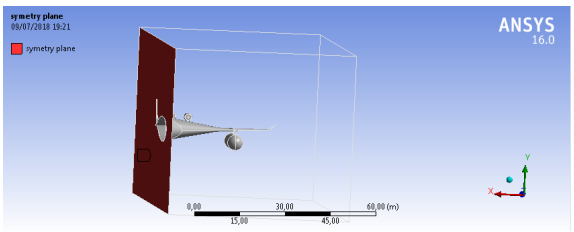

(c) Symmetry plane

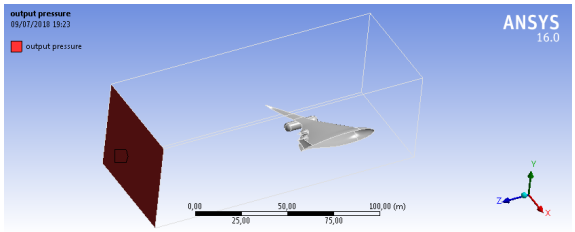

(b) Outlet named as Outputpressure

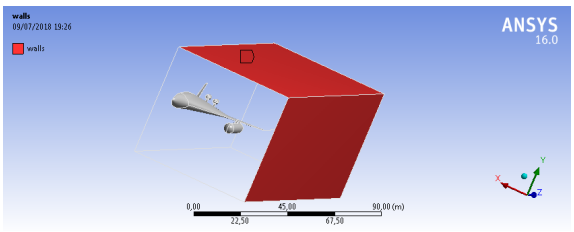

(d) Two of the three walls

Figure 5.2: Named Selections

5.2.2.. Mesh criteria

There are several parameters that modify the mesh configuration and thus the simulation conditions. Although CFD software packages have general mesh configurations by default, the automatic mesher is not suitable to perform aircraft simulations, due to its lack of accuracy and the complexity of the CAD files. The size criteria can be defined as ”fixed” or in function of ”Proximity”, ”Curvature” and ”Proximity and Curvature”.In this case, the best choice is ”Proximity and Curvature” due to the high complexity of the aircraft geometry and the lower complexity on the walls (boundary condition) proximities due to its simple shape (parallelepiped). The relevance center can be defined as ”Coarse”, ”Medium” and ”Fine”, depending on the desired accuracy. The best choice is ”Coarse”, since it is a tradeoff between significant computational cost and accuracy of the obtained results.

The minimum cell size as well as the body shape complexity have a strong influence on the successful convergence of the simulation run. The cell growth rate determines the size increase of the surrounding cells. Once the minimum and maximum cell size and the cell growth rate are set, this defines the number of cells in the mesh and their size on each region of the fluid domain. Usually, the higher the number of cells, the higher the use of PC memory and the higher the computational time, but a better accuracy and resolution of the results is obtained. Therefore, the PC characteristics limits the minimum cell size, etc.

As the geometry has a substantial complexity, the minimum cell size has also a maximum value, imposed by the size of the smallest features of the studied geometry. The chosen values for the mesh settings vary for the different studied aircrafts and control volumes. Although the requirements are fulfilled, the most problematic zones require a smaller cell size to perform a proper simulation. This can be accomplished with specific values for these settings affecting the mesh and total number of cells. Taking into account all the mentioned information, generally, a tradeoff between computational time and accuracy has to be considered. In this case, the selected minimum cell size is which gave the most accurate result at an affordable simulation time.

5.2.3.. Mesh quality check

The mesh configuration is an important issue in the simulation accuracy. When the generated mesh appears in black color, accomplishment of suitable mesh quality can be supposed. On the contrary, if the mesh appears in red color, the mesh quality is not sufficient, and then there are several parameters that help us improve the mesh quality. The Skewness criteria and an example of mesh quality results are shown in figure 5.3. Most of the points are within an acceptable range of skewness value, giving us an acceptable mesh.

Skewness is a face or cell indicator which determines the closeness to the ideal or desired case. This indicator can be from 0 (excellent) to 1 (inacceptable), as shown in figure 5.3a.In meshing, the best choices for cell element shape are equilateral or equiangular geometries, which have a skewness value of about 0. The point is that for complex geometries it is usually very difficult or impossible to make all the mesh using only such cell

elements.

The aspect ratio is the relationship between different geometry characteristic sizes of the cell elements. In our case, since we use tetrahedral cell shape, it can be defined as the ratio between the longest and the shortest edge. Generally, the coefficient must be lower than 40 but it can be tolerated up to 50 on the maximum inflation cells. An example of resulting aspect ratios is available in figures 5.3c and 5.3d.

The number of cells (Elements) is also available in figure 5.3c.

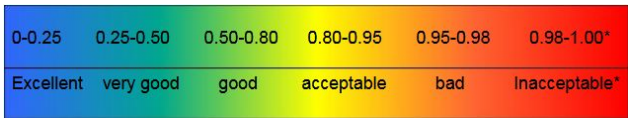

(a) skewness quality values criteria

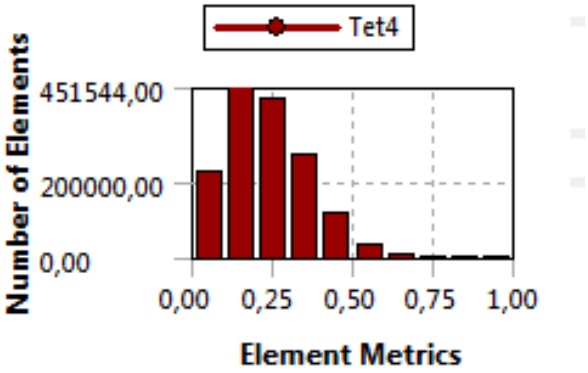

(b) Resulting skewness

Statistics	
Nodes	273977
Elements	1521674
Mesh Metric	Aspect Ratio
Min	1,1596
Max	45,787
Average	1,8504
Standard Deviation	0,51701

(c) Resulting Aspect ratio values

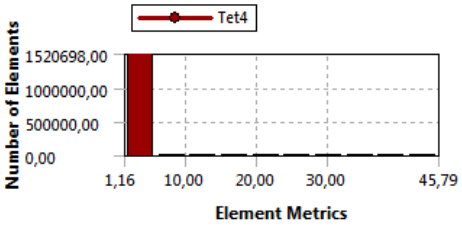

(d) Resulting Aspect ratio plot

Figure 5.3: Mesh quality check

5.3.. SETUP

In this section, the various settings of the solver will be explained. These parameters are dividedinto different menus, which can be observed in figure 5.4a. Although each menu includes different functionalities, this section is devoted to a general explanation of the set of configurations that are defined in Setup.

Several solver and physics model options can be selected. In our case, the problem will be defined as Pressure-based type, absolute velocity formulation and steady time [15] due to the available data and the time independence of our cruising flight. The flow characteristics on a CFD turbulent flow simulation is usually solved with the k-epsilon turbulence model. This model has been chosen due to its good convergence rate and relatively low memory requirements. Furthermore, it does perform well for external flow problems around complex geometries (such as aircrafts). The model uses principally two transport variables: the turbulent kinetic energy k, which is a measure of the energy in the turbulent flow, and

the turbulent dissipation e, which determines the rate of dissipation of the turbulent kinetic energy. The material and the state where by the aircraft goes through must be defined.

The normal or dynamic mesh can also be chosen, depeding on the possibility of a physical geometry change.As the aircraft is in a cruising flight (uniform rectilinear horizontal flight, with no transient state due to deployment of control surfaces or hyperlift devices), the conditions remain constant, so dynamic mesh (time-changing mesh) is not necessary.

Several characteristics and values of the boundary conditions must be defined. In our case, the ”input velocity” is defined as 252 $\frac{m}{s}$ (the supposed cruising speed of our BWB) and the Gauge pressure of the boundary condition ”output pressure” is defined as 0 Pa (away from the aircraft, the pressure of the fluid is equivalent to the atmospheric pressure).

For the CFD software to be able to compute the coefficients describing the aerodynamics performances (e.g., lift, drag, and pitching moment coefficient), some data must be provided, like the reference area, air density, and TAS. These parameters are named ”Reference Values”, and for computing the aerodynamic coefficients we need the fluid density, temperature and viscosity, and the aircraft wing layout area that can be computed with Ansys. As remarked previously, the density, viscosity and temperature are the corresponding to 11 km in ISA, i.e. 0.364 $\frac{kg}{m^3}$, 1.42e-05 $\frac{kg}{m \cdot s}$ and 216.65 K.

5.4.. SOLUTION

Before obtaining the simulation results, several settings must be defined relating to the solver. To perform a more accurate simulation, but at a higher computational cost, Coupled method, which couples the calculation of the pressure and velocity fields, has been defined. The Least Squares Cell Based gradient is used due to the tetrahedral cell shape, a common and quick type of cell element for meshing complex gemotries.

Regarding the gradient discretization, the best choice is PRESTO, which gives more accurate results since interpolation errors and pressure gradient assumptions on boundaries are avoided. The strong body forces and high Rayleigh number flows encourage the use of PRESTO. The Rayleigh number (Ra) of a fluid is a dimensionless number associated with the transfer of heat within the fluid. When the Rayleigh number is below a certain critical value, heat transfer occurs mainly by conduction; when it is above the critical value, heat transfer occurs mainly by convection. Finally, the Second order upwind solver has been selected in order to obtain an stable and accurate result.

The time of convergence and accuracy depend on several parameters that are also defined in this section. The Courant number(C) is the quotient between the time interval and the residence time in a finite volume. It is applied in the solution of differential equations in partial derivatives. It can be considered as a condition of convergence of differential equations in partial derivatives solved by certain algorithms, limiting the time interval bellow a given value. The Courant number has been set as 85 after testing several values. This value provides an accurate converged solution in a reasonable time. An example of the

simulation convergence is presented in the figures 5.4b and 5.4c. The number of iterations must also be defined, which establishes a maximum number of iterations that the computer is allowed to make to reach convergence before stop. In this case, given the complexity of the problem to be solved, the allowed number of iterations is large. As a reference of the computational cost resulted of the different choices, a simulation of 300 iterations it takes 1 hour and a half with the amount of elements in figure 5.3c, using a computer with an I7 processor, 8GB of RAM and a solid state drive of 120 GB.

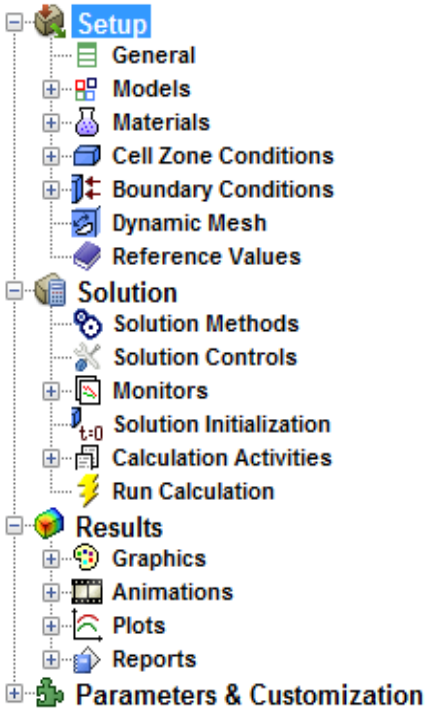

(a) Ansys menu

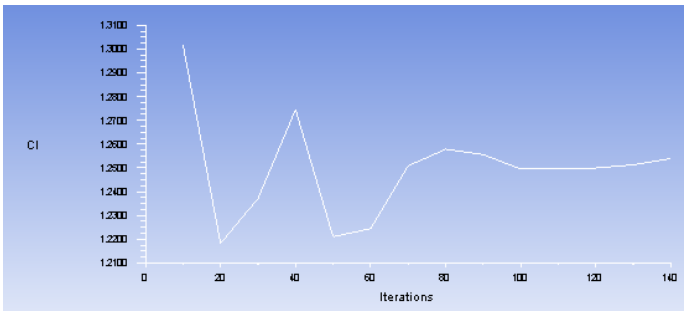

(b) cl convergence

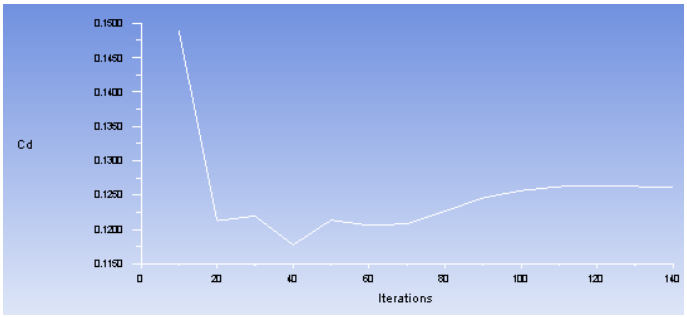

(c) cd convergence

Figure 5.4: Ansys menu (left) and examples of plots showing the convergence of Cl and Cd vs number of iterations (right)

CHAPTER 6. RESULTS AND DISCUSSION

First, a validation of the methods for obtaining performance parameters must be done. When all design factors concerning the aircrafts and hydrogen-realted implementations have been studied and validated, an analysis of the impact that the proposed solutions would have on the air transport industry is done. This section includes the several results on aerodynamic performance, aircraft masses and economic analysis, assuming a return trip LEBL-JFK (12600 km) and a return trip LEMD-LLBG (7200 km). In table 6.2 the kerosene has been considered as fuel. It must be taken into account that hydrogen consumption is a factor 2.8 smaller than kerosene consumption, due to the higher hydrogen specific energy or energy density.

6.1.. Comparison of results from CFD and empirical model

Once the drag results have been obtained from both methods (CFD and empirical model derived from BADA data), appropriate analysis of the results should done. The drag is the only parameter that has been calculated with both methods. The rest of the parameters come from CFD simulations and correlation of aircraft properties with surfaces, as already explained in the respective previous chapters. table 6.1 shows a comparison of the drag results from CFD and the empirical model derived from BADA data. The maximum difference in the drag obtained from these methods is 11.44%, for the case of the standard BWB. The error average and standard deviation are 9.75% and 1.37% respectively.

The results from the empirical model are always higher, so they are more conservative. Supposing the same wet surface, the friction drag of both, empirical and CFD results, must be equivalent. Thus, the difference could be origined due to the significant reduction of interference drag of the BWB in comparison with the drag tendence showed in conventional aircrafts [9].

In the case of giving a detriment in the empirical resulting drag, the thrust and fuel consumption would be less than necessary, so the empirical results would be more positive than the real ones. In systems with high levels of risk, more restrictive models are used due to its need for a high fault tolerance, so methods with a resulting drag lower than the real, can not be considered as suitable.

Aircraft model	drag from CFD (kN)	drag from BADA (kN)	Relative error
BWB_e V1	171.16	189.73	10.85%
BWB_e V2	170.20	189.67	11.44%
BWB_c	210.49	226.30	7.51%
BWB_{ci}	191.80	209.41	9.18%

Table 6.1: Comparison of drag results from CFD and from empirical model from BADA data

Although the drag results obtained from BADA data seem accurate, the lift has only been obtained from the CFD simulations. This can be done due to the assumption that the lift and MTOW depend on the wing layout area, being this a vertical projection of the wing surface that is not modified by the Kuchemann carrots implementation.

The fact that the results from both methods differ so little, allows us to use the empirical model with acceptable error, while requiring less computational cost and time. The impact of the Kuchemann carrots on the drag, consumption and OEW has been studied entirely with the developed empirical models. The MTOW is considered to be the same for the aircrafts with and without those anti-shock bodies. This is valid since presence of the Kuchemann carrots has barely no impact on the overall wing surface.

6.2.. Aerodynamic performance

Regarding the aerodynamic study, the efficiency of the BWB with ellipsoidal tanks (with and without modifying the original CAD file) is remarkable in relation with the rest of the BWB. Although, theoretically, BWB usually has a higher L/D ratio than conventional aircraft, the results show us otherwise. The aerodynamic efficiency is much lower than expected, due to the low lift coefficient. Observing Qin's research data [9], we can assume that this could be produced because of a wrong design performance (as wrong airfoil selection). Thus, probably, an accurate design would give us higher efficiency results.

The lift coefficients obtained for BWB are smaller than those of A380, which may give the wrong idea that BWB generate a much smaller lift compared to conventional aircraft. However, although the lift coefficients are smaller, as the BWB wing surface is much larger, BWB end up generating greater lift. The BWB drag coefficients are also smaller than those of A380, something that was expected, taking into account that the main characteristics of the BWB model are its greater wing surface, which is used to obtain the aerodynamic coefficients (being inversely proportional to these coefficients), and its reduction of total drag in comparison with the conventional aircrafts.

Aircraft model	Cl	Cd	E	Oil consumption
BWB_e V1	0.2253	0.0228	9.88	2.5810 $\frac{kg}{s}$
BWB_e V1(+)	-	-	-	2.6133 $\frac{kg}{s}$
BWB_e V2	0.2283	0.0229	9.97	2.5803 $\frac{kg}{s}$
BWB_e V2(+)	-	-	-	2.6126 $\frac{kg}{s}$
BWB_c	0.1882	0.0248	7.59	3.06$\frac{kg}{s}$
BWB_c (+)	-	-	-	3.0888$\frac{kg}{s}$
BWB_{ci}	0.1990	0.0238	8.36	2.8385 $\frac{kg}{s}$
BWB_{ci} (+)	-	-	-	2.8691 $\frac{kg}{s}$
A380	0.4821	0.0256	18.83	3.9785 $\frac{kg}{s}$

Table 6.2: Aerodynamic performance comparison; (+): corresponds to BWB with *Küchemann* Carrots

As expected, the c_l and c_d of the two BWBe models, on the one hand, and those of the BWBc models, on the other, are similar, but the c_l of the BWB_e V2 / BWB_{ci} is slightly higher than that of the BWB_e V1/BWB_c, probably due to the presence of a larger surface of external tanks, thus distorting the behavior of the flow in the wing environment. This argument also explains the reason why the c_l of the BWB_c models are about 15% smaller than those of the BWB_e.

Although a c_d of the BWB_c models was expected to be significantly greater than those of the BWB_e, they are only about 4% and 8% higher (BWB_e V2/BWB_e V1 compared to BWB_c/BWB_c respectively). The comparative results between the models with cylindrical tanks agree with what was expected; with the equality of wing layout area, the c_d of the BWB_{ci} is smaller than that of the BWB_c because the first eliminates the pylon that join the tanks to the wing.

Besides, the protruding caused by the ellipsoidal hydrogen tank implementation (BWB_e V1) does not produce a high affectation on the aerodynamic efficiency and fuel consumption. Hence, the fact that decreasing the range and increasing the efficiency may be better than otherwise, can be arguable in BWB_e implementation due to the considerable range decrease. Anyway, the trend of the aeronautical industry is improving the efficiency [16], so this small improvement in BWB efficiency could be worth in spite of the reduction in BWB range.

Finally, the superiority of the BWB_{ci} with respect to the BWB_c is clear in all aspects, even so, the full study has been done to show to show the effect of the pylons in aircraft performance.

6.3.. Aircraft masses

The larger wet area of the BWB with cylindrical tanks produces a substantial increase of the OEW (about 20 tones) in comparison with the BWB with ellipsoidal tank, but in any

case it is still lower than the OEW of the A380. Besides, the larger wing surface of the BWB with ellipsoidal tank (and the absence of cylindrical tanks in these BWB, which are blunt bodies that do not produce lift) provides a greater lift, which allows for a larger MTOW of these aircraft.

Aircraft model	Wet area (m^2)	OEW (T)	MTOW (T)
BWB_e V1	3051	160.31	2045.95
BWB_e V1(+)	3097.70	162.67	2045.95
BWB_e V2	3050	160.26	2270.49
BWB_e V2(+)	3096.70	162.62	2270.49
BWB_c	3778.2	197.01	2017.23
BWB_c (+)	3824.90	199.37	2017.23
BWB_{ci}	3432.09	179.54	2017.23
BWB_{ci} (+)	3478.79	181.90	2017.23
A380	5658.4	282.50	569

Table 6.3: Comparison of important aircraft masses; (+): corresponds to BWB with *Küchemann* Carrots.

The resulting MTOW allows us deduce that what will limit the aircraft takeoff weight will not be the capabilities of the aircraft, but those of the airport, like the maximum load bearing capacity of the pavement or the runway length. Even so, assuming an MTOW equivalent to that of the A380, the difference in OEW between the BWB_c and A380 enables 83 more tones of payload in the BWBc. Considering 105 kg per unit (passenger and luggage), 790 more passengers than A380 could be boarded in the BWBc, amount greater than what has been calculated in the previous cabin designs and, therefore, there would be no problems with the aircraft weights preventing the flight. Although assuming the tank mass add of table 6.4, the BWB designs continue to have, with their maximum capacity, a takeoff weight lower than the MTOW of the A380.

Aircraft model	Needed tank volume (m^3)	Tank mass (kg)
BWB_e V1	920.16	14743.43
BWB_e V1(+)	931.79	14880
BWB_e V2	920.01	14737.2
BWB_e V2(+)	931.55	14872
BWB_c	1091	4379.79
BWB_c (+)	1101.33	4422.89
BWB_{ci}	1012	4052.09
BWB_{ci} (+)	1022.99	4097.52

Table 6.4: Several tank volumes and masses to perform a flight of 15200 km; (+): corresponds to BWB with *Küchemann* Carrots

Regarding the tank volume needed to perform the respective flights, it is easy to see their direct relationship with the fuel consumption and efficiency. The higher consumption, the

larger the fuel mass and volume, introducing more complications to the tank integration or lesser aircraft efficiency. The ellipsoidal shape suppose a remarkable increase of the tank mass due to the adjustment of tank mass following figure 1.4. As the resulting regression OEW of cylindrical models are much higher, the BWB with ellipsoid hydrogen tank have lower structural weights.

6.4.. Economic analysis

If we want to perform an economic study, the Synjet and hydrogen price comparison must also be included due to their relevance on the aircraft DOC. The Synjet price evolution during the last year is captured in Fig. 6.1. The Jet Fuel Price Index is the current value of Jet fuel price, converted to USD and expressed as a percentage of the average price for the base period (2000). Actually, 100 in 2000 corresponds to 87 cts/gal, and thus, for instance, for the index 246.6, the actual cost would be obtained multiplying 0.87 by 246.6; in this case, 711.3 $ per metric tone. The hydrogen price has also been studied. The type of electrolysis, transportation, liquefying and LH_2 demand are factors which have a substantial influence on the hydrogen costs. As the hydrogen economy depends on several parameters, many example prices have been found.

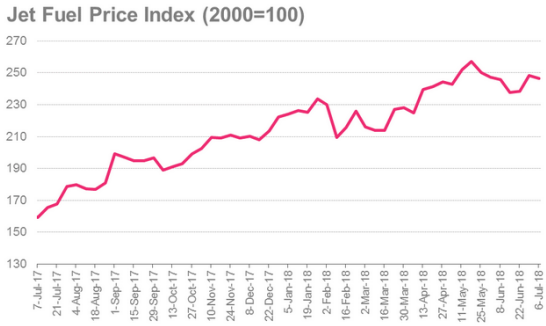

Figure 6.1: Synjet fuel price evolution from July 2017 to July 2018 [17]

The initial investment, like vehicles and infrastructure for electrolysis or liquefying, has not been taken into account in the hydrogen and Synjet prices. The production cost of a clean electrolysis is about $3.8\frac{\$}{kgH_2}$ [18].
A coming market also should be studied. In reference [19], a hydrogen price below 4$/gge is expected for 2020. Assuming the predictions are fulfiled, an increase of the total benefits can be supposed.

Note that one gge is the amount of alternative fuel necessary to equal the energy content of one liquid gallon of gasoline. One gallon corresponds to 3.785 L. Taking into account the fact that 2.8 kg of kerosene produces the same amount of energy than 1 kg of LH2, and the kerosene density of 0.8 kg/L, the price can be calculated as Eq. 6.1.

$$P = 4\$/gge \cdot \frac{1galon}{3.785L} \cdot \frac{1L}{0.812kg} \cdot \frac{2.8kgkerosene}{1kgH_2} = \frac{3.64\$}{kgH_2} \tag{6.1}$$

The storage and transportation produces an increases on the total price which it will categoryzed into two possibilities: the best and the worst case scenario. The lower distance from the supplier and the higher production amount per hour, the lower added price. The best case scenario is when the hydrogen production infrastructures are close to the airport and there is demand for high production rates. The worst case scenario is when the hydrogen production infrastructures are far from the airport there is demand for high production rate. Note that both scenarios are based on the assumption of high production rate, due to the general large demand of fuel from airports, especially where high capacity aircrafts are used.

An example can be the LEBL airport, which has a capacity of 90 flights per hour and a mean of 68 flights per hour [20].An analysis of the traffic on July 15, 2018, has been performed in order to extract an approximation of the the hourly demand of fuel from the airport. The traffic oscillates during the day, as shown in table 6.5, which only includes traffic from 6 to 24h, as the number of flights until 6h is negligible.

Time interval	Number of departures	Time interval	Number of departures
From 6 to 7	80	From 15 to 16	49
From 7 to 8	80	From 16 to 17	61
From 8 to 9	37	From 17 to 18	65
From 9 to 10	43	From 18 to 19	60
From 10 to 11	68	From 19 to 20	48
From 11 to 12	89	From 20 to 21	74
From 12 to 13	80	From 21 to 22	42
From 13 to 14	45	From 22 to 23	44
From 14 to 15	61	From 23 to 00	18

Table 6.5: Departures during July 15, 2018 [21]

The hourly demand of fuel from the airport has been calculated from the 43 departures between 9 and 10h. The amount of fuel has been calculated with Eq. 6.2 taking into account the data of table 6.6.

Aircraft model	Number of departures	Flight time (t_i)	Consumption (C_i)
A310	1	164 min	1.67 $\frac{kg}{s}$
A319	7	781 min	0.66 $\frac{kg}{s}$
A320	22	2250 min	0.74 $\frac{kg}{s}$
A321	7	736 min	0.84 $\frac{kg}{s}$
B737-800	3	390 min	0.74 $\frac{kg}{s}$
CRJ-200	2	186 min	0.3 $\frac{kg}{s}$
A350-900	2	1278 min	2.79 $\frac{kg}{s}$

Table 6.6: Aircraft characteristics of the departures during July 15, 2018 from 9AM to 10AM [21](Prat Salidas)

$$C_A = \sum_{i=1}^{N_f} C_i \cdot t_i = 418849.11 kg/h \tag{6.2}$$

Supposing hydrogen instead of kerosene, the C_A is reduced up to 149588.97 kg per hour, which is higher than the 4500 kg per hour of the article [22], allowing us to use the same prices.

The study performed in reference [22], in addition to our particular assumptions, results on an added price of $0.5 \frac{\$}{kgH_2}$ in the best case and $0.9 \frac{\$}{kgH_2}$ in the worst case, resulting in final prices of 4.3 and 4.7 $\frac{\$}{kgH_2}$. For the case of near market, the prices for the best and worst case, are 4.14 and 4.54 $\frac{\$}{kgH_2}$, respectively.

The assumed flight ticket prices, necessary for conducting the economic analysis, have been fixed according to Lufthansa LEBL-JFK rates as shown in table 6.7 and Iberia LEMD-LLBG rates as shown in table 6.8.

type of seat	Price €	Width (m)	Depth (m)
First Class	4410	0.58	2.28
Business	2650	0.47	1.32
Economy	650	0.46	0.91

Table 6.7: Lufthansa LEBL-JFK prices and seat conditions for the several passenger classes

type of seat	Price €	Width (m)	Depth (m)
Business	1100	0.58	2.10
Economy Premium	800	0.47	1.04
Economy	500	0.46	0.91

Table 6.8: Iberia LEMD-LLBG prices and seat conditions for the several passenger classes

Finally, the benefit (i.e., the difference between the gains obtained from transporting the payload and the fuel expenses) of the return trip LEBL-JFK has been calculated in tables 6.9 6.10 6.11 for the studied BWB designs in the best and worst current and future hydrogen prices scenarios, without taking into account other economic factors as the workers' salary, profit from suitcases or restoration in order to simplify the problem.

	Best scenario (3.66 €/kg)			Worst scenario (4 €/kg)		
Aircraft model	**Fuel expense**	**Gain**	**Benefit**	**Fuel expense**	**Gain**	**Benefit**
BWB_{ci}	185.52	613.08	466.36	202.50	613.08	449.38
BWB_c	199.99	613.08	451.89	218.30	613.08	433.58
BWB_e V1.30	168.69	459.32	290.63	184.13	459.32	275.19
BWB_e V2.30	168.64 k	459.32	290.68	184.08	459.32	275.24
BWB_{ci}(+)	187.52	613.08	464.36	204.68	613.08	447.20
BWB_c (+)	201.88	613.08	450	220.35	613.08	431.53
BWB_e V1.30 (+)	170.80	459.32	288.52	186.430	459.32	272.89
BWB_e V2.30 (+)	170.75	459.32	288.57	186.38	459.32	272.94

Table 6.9: Benefits of return trip LEBL-JFK in k€ with the studied BWB designs with best and worst current hydrogen prices scenario; (+): corresponds to BWB with $Küchemann$ Carrots

	Best scenario (3.51 €/kg)			Worst scenario (3.85 €/kg)		
Aircraft model	**Fuel expense**	**Gain**	**Benefit**	**Fuel expense**	**Gain**	**Benefit**
BWB_{ci}	177.91	613.08	473.97	195.60	613.08	456.28
BWB_c	191.80	613.08	460.08	210.87	613.08	441.01
BWB_e V1.30	161.77	459.32	297.55	177.86	459.32	281.46
BWB_e V2.30	161.73	459.32	297.59	177.81	459.32	281.51
BWB_{ci} (+)	179.83	613.08	472.05	197.71	613.08	454.17
BWB_c (+)	193.60	613.08	458.28	212.85	613.08	439.03
BWB_e V1.30 (+)	163.80	459.32	295.52	180.08	459.32	279.24
BWB_e V2.30(+)	163.75	459.32	295.57	180.04	459.32	279.28

Table 6.10: Benefits of return trip LEBL-JFK in k€ with the studied BWB designs with best and worst future hydrogen prices scenario; (+): corresponds to BWB with $Küchemann$ Carrots

	Actual oil price (0.587 €/kg)		
Aircraft model	**Fuel expense**	**Gain**	**Benefit**
A380	116.77	530.85	414.08
A340-600	85.18	412.11	326.93
A340-300	64.86	266.43	201.57
A330-300	49.40	340.84	291.44

Table 6.11: Benefits of return trip LEBL-JFK in k€ with conventional kerosene-fuelled aircraft with the current oil scenario

The current difference between kerosene and hydrogen prices does not prevent having good economic results. Observing the results for the LEBL-JFK flight, it is clear that the BWB with integrated hydrogen tanks is a potential substitute for the A380, in the same way that the BWB with ellipsoidal hydrogen tank is a potential substitute for the A340-600.

Although the BWB with ellipsoidal tank is the most efficient design in terms of L/D ratio, it is not the most economically profitable in the studied flight due to its low capacity in passengers. However, it could show better profitability results in shorter flights. The BWB with cylindrical tanks may have too much capacity to fly with high occupancy of passengers in shorter flights, and, besides, it has a higher fuel consumption. Thus, in the same way that happens with the A380, it may be less profitable in these cases.

The benefit (i.e., the difference between the gains obtained from transporting the payload and the fuel expenses) of the return trip LEMD-LLBG has been calculated in tables 6.12 6.13 6.14 for the studied BWB designs in the best and worst current and future hydrogen prices scenarios.

	Best scenario (3.66 €/kg)			**Worst scenario (4 €/kg)**		
Aircraft model	**Fuel expense**	**Gain**	**Benefit**	**Fuel expense**	**Gain**	**Benefit**
BWB_e V1.31	96.39	257.60	161.21	105.22	257.60	152.38
BWB_e V1.21	96.39	270	173.61	105.21	270	164.78
BWB_e V2.31	96.37	257.60	161.23	105.19	257.60	152.42
BWB_e V2.21	96.37	270	173.63	105.19	270	164.81
BWB_e V2.22	96.37	237.60	141.23	105.19	237.60	132.41
BWB_e V1.31 (+)	97.60	257.60	160	106.53	257.60	151.07
BWB_e V1.21 (+)	97.60	270	172.40	106.53	270	163.47
BWB_e V2.31 (+)	97.57	257.60	160.03	106.50	257.60	151.10
BWB_e V2.21 (+)	97.57	270	172.43	106.50	270	163.50
BWB_e V2.22 (+)	97.57	237.60	140.03	106.50	237.60	131.10

Table 6.12: Benefits of return trip LEMD-LLBG in k€ with the studied BWB designs with best and worst current hydrogen prices scenario; (+): corresponds to BWB with *Küchemann* Carrots

	Best scenario (3.51 €/kg)			**Worst scenario (3.85 €/kg)**		
Aircraft model	**Fuel expense**	**Gain**	**Benefit**	**Fuel expense**	**Gain**	**Benefit**
BWB_e V1.31	92.44	257.60	165.16	101.63	257.60	155.97
BWB_e V1.21	92.44	270	177.56	101.63	270	168.37
BWB_e V2.31	92.42	257.60	165.18	101.61	257.60	155.99
BWB_e V2.21	92.42	270	177.58	101.61	270	168.39
BWB_e V2.22	92.42	237.60	145.18	101.61	237.60	135.99
BWB_e V1.31(+)	93.60	257.60	164	102.91	257.60	154.69
BWB_e V1.21 (+)	93.60	270	176.40	102.91	270	167.09
BWB_e V2.31 (+)	93.57	257.60	164.03	102.88	257.60	154.72
BWB_e V2.21 (+)	93.57	270	176.43	102.88	270	167.12
BWB_e V2.22 (+)	93.57	237.60	144.03	102.88	237.60	134.72

Table 6.13: Benefits of return trip LEMD-LLBG in k€ with the studied BWB designs with best and worst future hydrogen prices scenario; (+): corresponds to BWB with *Küchemann* Carrots

	Actual kerosene price (0.587 €/kg)		
Aircraft model	**Fuel expense**	**Gain**	**Benefit**
A340-600	48.67	206	157.33
A340-300	37.06	128.4	91.34
A330-300	28.23	169.7	141.47
A330-200	29.73	155.4	125.67
A320-200	13.59	96	82.41
A310	29.86	122	92.14

Table 6.14: Benefits of return trip LEMD-LLBG in k€ with conventional kerosene-fuelled aircraft with the current oil scenario

Similarly to LEBL-JFK results,the hydrogen-powered BWB would generate benefits comparable to those of the conventional kerosene-fuelled aircraft, even in the worst case hydrogen price scenario. The choice of aircraft configuration is not only based on the economic study, but also on demand. Thus, between the different models in table 6.13, despite the remarkable result of BWB_e V1.21 and BWB_e V2.21, there is not a perfect choice for all situations. Furthermore, the origin and destination airports must afford the operation of aircrafts with 80 m of wingspan.

CONCLUSIONS

The main worldwide energy sources come from fossil origins, generating therefore pollution. The current aircrafts engines are mainly powered by Synjet (kerosene), a fossil fuel that will have to be abandonned in a few years to mitigate climate change. As a follow up of previous investigations,, hydrogen has been proposed to replace the kerosene, reducing drastically the air transport pollution.

The low density of LH_2 implies complications on the integration of the hydrogen tank(s) in the aircraft, which lead us to search alternative aircraft configurations that allow maintaining the current worlwide air traffic without being drastically detrimental on the aircraft consumption or aerodynamic performances. The non-conventional BWB has been selected due to its great aerodynamic performance and its large volume per wet surface ratio.

A configuration with two cylindrical tanks implemented in conventional wing positions has been proposed, increasing the aircraft fuel consumption but enabling a large quantity of passengers onboard and an aircraft range of 15200 km.
A configuration with two ellipsoidal tanks implemented in conventional positions on top of the fuselage has also been proposed, improving the aerodynamic performances but decreasing the passenger capacity. Two different ranges (15200 and 11400 km) have been studied for this configuration. The design process finishes with different interior designs of the passenger cabin to compute the aircraft capacity.

In order to study the aerodynamic behavior of the several models, two different methods have been used and compared. First a CFD simulation of each aircraft design has been done, obtaining the lift and drag forces and coefficients.
Another method has been proposed, which is based on our theoretical knowledge on aerodynamics and flight mechanics, and on information from BADA. From this, we proposed an empirical model: a set of equations that allow us calculate the drag, fuel consumption, MTOW and OEW as a function of wing and wet surfaces.

The aircraft models with cylindrical tanks show more similarity in the results obtained from both methods, likely because the empirical model has been developed from data from conventional aircrafts, which have a blunt body (their fuselage), and the external cylindrical tanks are also blunt bodies causing similar phenomena. Conversely, in the aircraft configurations with ellipsoidal tanks, there are no equivalent blunt bodies (the tanks are encapsulated within the BWB), and the difference in the drag obtained from CFD and the empirical model is larger likely due to the error in the estimated induced drag and interference drag. That is, the drag obtained from the empirical model is larger than that from CFD simulations (that we assume to be closer to reality) because it comes from regressions from data for historical aircraft that have interference drag, blunt parts, and which on top need larger lift coefficients (leading thus to larger induced drag) due to their smaller wing layout surface compared to the BWB.

The validation of the second method enables its use, saving the CFD time. Thus, the em-

pirical model has been used to quantify the Kuchemann carrot impact on several parameters. The analysis of the results can be divided in masses, aerodynamic and economic sections.

The aicraft masses results include the several parameters that are involved on the aircraft structure. The important aicraft masses that we analyzed are OEW and MTOW. The use of BWB would suppose a decrease of the structural weight due to its lower wet surface per volume ratio. Thus, supposing the same A380 MTOW, there would be no overweight problems. Furthermore, the high lift from the BWB allows the aircraft to carry much more weight in a cruise flight (the denominated MTOW in the tables) so, probably, the aircraft weight limitations would only be defined by the airport characteristics.

Regarding the aerodynamics,the lift coefficients obtained for the BWB are lower than expected, but this does not penalize the lift force because the lower lift coefficients of the BWB are compensated by their larger wing surface. The drag coefficients are lower than those for the A380, as expected, since the BWB has less blunt parts and no intereference drag. The obtained L/D ratios for the studied BWB are smaller than expected, leading us to conclude that the design we used is not optimum. Even so, according to the results, the higher drag force given by the empirical equation exceeds the drag obtained from CFD, which give us to conclude the substantial reduction of the drag which implies the BWB geometry. Nevertheless, even assuming the worst case scenario, the modified BWBs still have better fuel consumption per passenger rate, i.e, for a given fuel consumption rate, the BWB could accommodate more passengers than other conventional commercial aircraft.

Despite the exorbitant price of hydrogen compared to Synjet and the inefficiencies or losses of available space in the aircraft produced by the implementation of hydrogen, the high energy density of hydrogen and the great qualities of the BWB lead to economic results comparable to the current conventional aircrafts. Furthermore, a future decrease of the hydrogen price can be expected, due to the increase in demand and the improvement of electrolysis technologies. Thus, the implementation of improved hydrogen powered BWBs in the airspace, followed by the hydrogen price decrease would imply the increase of the airline profits or a decrease of the ticket prices.

The incorporation of Kuchemann carrots is essential to avoid problems and inefficiencies produced by shock waves. The maximum changes are the BWB_e fuel consumption increase of 1.25% and the BWB_c OEW increase of 1.85%. Based on the different results, we can conclude that it does not produce a critical detriment of the aircraft behavior. Finally, the aviation tendency of increasing the aerodynamic performances to reduce the fuel consumption could be prioritized over improving other parameters such as the range or economic results, thus favoring the use of BWB with ellipsoidal tanks. Anyway, the feasibility of these implementations depends on many factors, including airport runways, which, except for the most frequented, may have problems to accommodate aircrafts of this size.

BIBLIOGRAPHY

[1] A. Contreras, S. Yiğit, K. Özay, and T. Veziroğlu, "Hydrogen as aviation fuel: a comparison with hydrocarbon fuels," *International Journal of Hydrogen Energy*, vol. 22, no. 10-11, pp. 1053–1060, 1997.

[2] G. McTaggart-Cowan, S. Munshi, S. Rogak, P. Hill, and W. Bushe, "Hydrogen-methane blend fuelling of a heavy-duty, direct-injection engine," in *ASME 2007 International Mechanical Engineering Congress and Exposition*, pp. 521–530, American Society of Mechanical Engineers, 2007.

[3] G. Corchero and J. Montanes, "An approach to the use of hydrogen for commercial aircraft engines," *Proceedings of the Institution of Mechanical Engineers, Part G: Journal of Aerospace Engineering*, vol. 219, no. 1, pp. 35–44, 2005.

[4] C. Winnefeld, T. Kadyk, B. Bensmann, U. Krewer, and R. Hanke-Rauschenbach, "Modelling and designing cryogenic hydrogen tanks for future aircraft applications," *Energies*, vol. 11, no. 1, p. 105, 2018.

[5] B. C. Airplanes, "Airplane characteristics for airport planning," 2013.

[6] A. J. Colozza and L. Kohout, "Hydrogen storage for aircraft applications overview," 2002.

[7] H. W. Pohl and V. V. Malychev, "Hydrogen in future civil aviation," *International journal of hydrogen energy*, vol. 22, no. 10-11, pp. 1061–1069, 1997.

[8] A. K. Sehra and W. Whitlow Jr, "Propulsion and power for 21st century aviation," *Progress in Aerospace Sciences*, vol. 40, no. 4-5, pp. 199–235, 2004.

[9] N. Qin, A. Vavalle, A. Le Moigne, M. Laban, K. Hackett, and P. Weinerfelt, "Aerodynamic considerations of blended wing body aircraft," *Progress in Aerospace Sciences*, vol. 40, no. 6, pp. 321–343, 2004.

[10] J. B. Chang, *Damage tolerance of metallic structures: Analysis methods and applications*. ASTM International, 1984.

[11] C. Schwarz, K.-U. Hahn, and D. Fischenberg, "Wake encounter severity assessment based on validated aerodynamic interaction models," in *AIAA Atmospheric and Space Environments Conference*, p. 7679, 2010.

[12] K.-U. Hahn, C. Schwarz, and H. Friehmelt, "A simplified hazard area prediction (shape) model for wake vortex encounter avoidance," in *24th International Congress of Aeronautical Sciences, Yokohama (Japan)*, vol. 29, 2004.

[13] W. K. Abeyounis and J. C. Patterson Jr, "Effect of underwing aft-mounted nacelles on the longitudinal aerodynamic characteristics of a high-wing transport airplane," 1985.

[14] J. B. Barlow, W. H. Rae, and A. Pope, "Low-speed wind tunnel testing," 1999.

[15] E. Lopez Castillo and X. Paricio Vallespi, "Analysis of the effect of large fuel tanks on aerodynamic performances of heavy trucks and large aircraft," B.S. thesis, Universitat Politècnica de Catalunya, 2017.

[16] T. Ferrer and E. P. Sandro Pozzi, “Aviones que van mas lejos a menor coste.” urlhttps://elpais.com/economia/2018/04/06/actualidad/1523026887_055266.html.

[17] IATA, “Jet fuel price monitor.” urlhttps://www.iata.org/publications/economics/fuel-monitor/Pages/index.aspx.

[18] R. Ahluwalia, J. Peng, T. Hua, and C. C. Marriott, “Cryo-compressed hydrogen storage: Performance and cost review,” in *R&D strategies for compressed, cryo-compressed and cryo-sorbent hydrogen storage technologies workshops on February*, vol. 14, 2011.

[19] S. Satyapal, “Us department of energy hydrogen and fuel cell overview,” 2016.

[20] L. V. David Guerrero, “El aeropuerto de el prat vuela hacia el límite de su capacidad.” urlhttps://www.lavanguardia.com/local/barcelona/20161113/411819362286/aeropuerto-el-prat-limite-capacidad.html, 2017.

[21] A. B.-E. Prat, “Salidas barcelona el prat (bcn-lebl).” urlhttps://www.aeropuertobarcelona-elprat.com/cast/salidas-aeropuerto-barcelona.html.

[22] W. A. Amos *et al.*, *Costs of storing and transporting hydrogen*. National Renewable Energy Laboratory Golden, CO, 1998.

[23] E. Torenbeek, *Synthesis of subsonic airplane design: an introduction to the preliminary design of subsonic general aviation and transport aircraft, with emphasis on layout, aerodynamic design, propulsion and performance*. Springer Science & Business Media, 2013.

[24] B. Mialon, T. Fol, and C. Bonnaud, “Aerodynamic optimization of subsonic flying wing configurations,” in *20th AIAA applied aerodynamics conference*, p. 2931, 2002.

[25] M. E. G. Sánchez, “Principales técnicas de almacenamiento de hidrógeno,” *Marzo del*, 2003.

[26] C. Yang and J. Ogden, “Determining the lowest-cost hydrogen delivery mode,” *International Journal of Hydrogen Energy*, vol. 32, no. 2, pp. 268–286, 2007.

[27] A. Pino Priego, “Aprovechamiento de recursos energéticos renovables no integrables en la red eléctrica. el caso de la producción de hidrógeno,” B.S. thesis, ESCUELA TÉCNICA SUPERIOR DE INGENIEROS DE SEVILLA, 2009.

[28] P. W. Civera, “Condiciones ergonómicas durante el trayecto en avión en clase turista,” B.S. thesis, Tesina, 2011.

[29] A. Fluent, “14.5, theory guide; ansys,” *Inc., Canonsburg, PA*, 2012.

APPENDICES

APPENDIX A. INTERNATIONAL STANDARD ATMOSPHERE (ISA)

The International Standard Atmosphere (ISA) is a reference atmosphere defined by the International Civil Aviation Organization (ICAO), under the umbrella of the United Nations (UN). Namely, ICAO elaborates international regulations and recommendations to guarantee the safety, security, efficiency and regularity of the air transport and acts as a catalyst for the cooperation between its contracting states in all the spheres of civil aviation. ICAO states the following four characteristics to define ISA:

1. The established conditions (reference values) for ISA at zero altitude or Sea Level (SL) are the following:

a. Static pressure: $p_0 = p_{SL} = 1013.25$ mb
b. Temperature: $T_0 = T_{SL} = 15$ºC $= 288.15$ K
c. Density: $\rho_0 = \rho_{SL} = 1.225$ kg/m^3

2. ISA temperature vs. height profile is defined as shown in Fig. A.1:

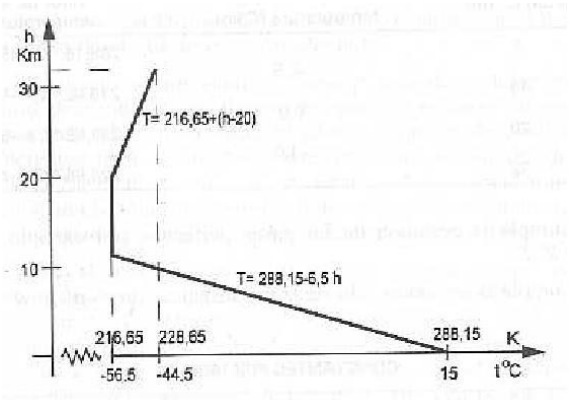

Figure A.1: Plot of Temperature [C and K] vs. Height [km] for the ISA.

3. Air in ISA behaves as a perfect gas (i.e. ISA is compliant with the perfect gases equation):
Equation 1 $\frac{p}{\rho} = R'_a \cdot T$

4. ISA is compliant with the fluid statics law:
Equation 2 $dp = -\rho \cdot g \cdot dh$

Reference:
Carmona, A.I., Aerodinámica y Actuaciones del Avión, 12th ed., Editorial Paraninfo, Madrid, Spain, 2004

APPENDIX B. INTERIOR DESIGNS

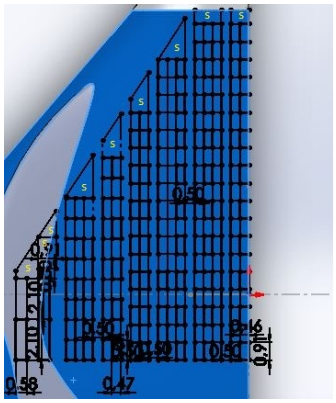

Figure B.1: BWB_e 3 class configuration: economy, economy premium and business

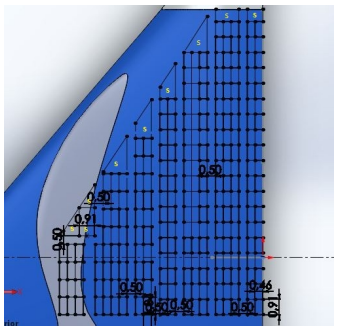

Figure B.2: BWB_e 2 class configuration: economy and business

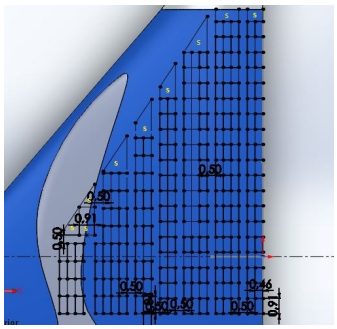

Figure B.3: BWB_e 2 class configuration: economy and economy premium

APPENDIX C. BADA REGRESSION CODE

```
%310
model310204='A310-204';
model310222='A310-222';
model310308='A310-308';
model310322='A310-322';
model310324='A310-324';

W310204=givemeW(model310204);
W310222=givemeW(model310222);
W310308=givemeW(model310308);
W310322=givemeW(model310322);
W310324=givemeW(model310324);

wetarea310=759.349*2;
% wetarea310222=;
% wetarea310308=;
% wetarea310322=;
% wetarea310324=;

Vcruc310=236.111; %850 km/h

[D310204,F310204]=Calculateconsumption(model310204,Vcruc310);
[D310222,F310222]=Calculateconsumption(model310222,Vcruc310);
[D310308,F310308]=Calculateconsumption(model310308,Vcruc310);
[D310322,F310322]=Calculateconsumption(model310322,Vcruc310);
[D310324,F310324]=Calculateconsumption(model310324,Vcruc310);

D310(1)=D310204;
D310(2)=D310222;
D310(3)=D310308;
D310(4)=D310322;
D310(5)=D310324;

D310=max(D310);

F310(1)=F310204;
F310(2)=F310222;
F310(3)=F310308;
F310(4)=F310322;
F310(5)=F310324;

F310=max(F310);

W310(1)=W310204;
W310(2)=W310222;
```

```
W310(3)=W310308;
W310(4)=W310322;
W310(5)=W310324;

W310=max(W310);

%319
model319114='A319-114';
model319131='A319-131';

Vcruc319=230; %828 km/h

[D319114,F319114]=Calculateconsumption(model319114,Vcruc319);
[D319131,F319131]=Calculateconsumption(model319131,Vcruc319);

F319(1)=F319114;
F319(2)=F319131;

F319=max(F319);
%321
model321111='A321-111';
model321131='A321-131';

Vcruc321=230; %828 km/h

[D321111,F321111]=Calculateconsumption(model321111,Vcruc321);
[D321131,F321131]=Calculateconsumption(model321131,Vcruc321);

F321(1)=F321111;
F321(2)=F321131;

F321=max(F321);
%320
model320212='A320-212';
model320214='A320-214';
model320231='A320-231';
model320232='A320-232';

W320212=givemeW(model320212);
W320214=givemeW(model320214);
W320231=givemeW(model320231);
W320232=givemeW(model320232);

wetarea320=479.34*2;
% wetarea320214=;
% wetarea320231=;
% wetarea320232=;

```

```
94  Vcruc320=230; %828 km/h
95
96  [D320212,F320212]=Calculateconsumption(model320212,Vcruc320);
97  [D320214,F320214]=Calculateconsumption(model320214,Vcruc320);
98  [D320231,F320231]=Calculateconsumption(model320231,Vcruc320);
99  [D320232,F320232]=Calculateconsumption(model320232,Vcruc320);
100
101 D320(1)=D320212;
102 D320(2)=D320214;
103 D320(3)=D320231;
104 D320(4)=D320232;
105
106 D320=max(D320);
107
108 F320(1)=F320212;
109 F320(2)=F320214;
110 F320(3)=F320231;
111 F320(4)=F320232;
112
113
114 F320=max(F320);
115
116 W320(1)=W320212;
117 W320(2)=W320214;
118 W320(3)=W320231;
119 W320(4)=W320232;
120
121
122 W320=max(W320);
123
124 %330-200
125 model330203='A330-203';
126 model330223='A330-223';
127 model330243='A330-243';
128
129 W330203=givemeW(model330203);
130 W330223=givemeW(model330223);
131 W330243=givemeW(model330243);
132
133 wetarea330=1332.792*2;
134 % wetarea330223=;
135 % wetarea330243=;
136
137 Vcruc330=241.994; %871 km/h
138
139 [D330203,F330203]=Calculateconsumption(model330203,Vcruc330);
140 [D330223,F330223]=Calculateconsumption(model330223,Vcruc330);
141 [D330243,F330243]=Calculateconsumption(model330243,Vcruc330);
```

```
142
143
144 %330-300
145 model330301='A330-301';
146 model330321='A330-321';
147 model330341='A330-341';
148
149 W330301=givemeW(model330301);
150 W330321=givemeW(model330321);
151 W330341=givemeW(model330341);
152
153 % wetarea330301=;
154 % wetarea330321=;
155 % wetarea330341=;
156
157 [D330301,F330301]=Calculateconsumption(model330301,Vcruc330);
158 [D330321,F330321]=Calculateconsumption(model330321,Vcruc330);
159 [D330341,F330341]=Calculateconsumption(model330341,Vcruc330);
160
161 D330(1)=D330203;
162 D330(2)=D330223;
163 D330(3)=D330243;
164 D330(4)=D330301;
165 D330(5)=D330321;
166 D330(6)=D330341;
167
168 D330=max(D330);
169
170 F330(1)=F330203;
171 F330(2)=F330223;
172 F330(3)=F330243;
173 F330(4)=F330301;
174 F330(5)=F330321;
175 F330(6)=F330341;
176
177 F330=max(F330);
178
179 W330(1)=W330203;
180 W330(2)=W330223;
181 W330(3)=W330243;
182 W330(4)=W330301;
183 W330(5)=W330321;
184 W330(6)=W330341;
185
186 W330=max(W330);
187 %340
188 model340213='A340-213';
189 model340313='A340-313';
```

```
model340541='A340-541';
model340642='A340-642';

W340213=givemeW(model340213);
W340313=givemeW(model340313);
W340541=givemeW(model340541);
W340642=givemeW(model340642);

wetarea340=1411.010738*2;
% wetarea340313=;
% wetarea340541=;
% wetarea340642=;

Vcruc340=241.994; %871 km/h

[D340213,F340213]=Calculateconsumption(model340213,Vcruc340);
[D340313,F340313]=Calculateconsumption(model340313,Vcruc340);
[D340541,F340541]=Calculateconsumption(model340541,Vcruc340);
[D340642,F340642]=Calculateconsumption(model340642,Vcruc340);

D340(1)=D340213;
D340(2)=D340313;
D340(3)=D340541;
D340(4)=D340642;

D340=max(D340);


F340(1)=F340213;
F340(2)=F340313;
F340(3)=F340541;
F340(4)=F340642;

F340=max(F340);

W340(1)=W340213;
W340(2)=W340313;
W340(3)=W340541;
W340(4)=W340642;

W340=max(W340);
%380
model380841='A380-841';
model380861='A380-861';

Vcruc380=252; %907 km/h

W380841=givemeW(model380841);
```

```
W380861=givemeW(model380861);

wetarea380=2829.196*2;
% wetarea380861=;

[D380861,F380861]=Calculateconsumption(model380841,Vcruc380);
[D380841,F380841]=Calculateconsumption(model380861,Vcruc380);

D380(1)=D380861;
D380(2)=D380841;


D380=max(D380);

F380(1)=F380861;
F380(2)=F380841;


F380=max(F380);

W380(1)=W380861;
W380(2)=W380841;


W380=max(W380);

D(1)=D310;
D(2)=D320;
D(3)=D330;
D(4)=D340;
D(5)=D380;

F(1)=F310;
F(2)=F320;
F(3)=F330;
F(4)=F340;
F(5)=F380;

W(1)=W310;
W(2)=W320;
W(3)=W330;
W(4)=W340;
W(5)=W380;

A(1)=wetarea310;
A(2)=wetarea320;
A(3)=wetarea330;
A(4)=wetarea340;
```

```
A(5)=wetarea380;

scatter(A,D);
%Standard Kucheman
wetareaBWBsk=3050+46.704;


VcrucBWBsk=Vcruc380;

FBWBsk=CalculateconsumptionBWB(wetareaBWBsk);
OEWBWBsk=CalculateOEWBWB(wetareaBWBsk);
DBWBsk=CalculateDBWB(wetareaBWBsk);

%Ellipsoid kucheman
wetareaBWBek=3051+46.704;


VcrucBWBek=Vcruc380;

FBWBek=CalculateconsumptionBWB(wetareaBWBek);
OEWBWBek=CalculateOEWBWB(wetareaBWBek);
DBWBek=CalculateDBWB(wetareaBWBek);

%Cylindrical integrated kucheman
wetareaBWBcik=3432.09+46.704;


VcrucBWBcik=Vcruc380;

FBWBcik=CalculateconsumptionBWB(wetareaBWBcik);
OEWBWBcik=CalculateOEWBWB(wetareaBWBcik);
DBWBcik=CalculateDBWB(wetareaBWBcik);

%Cylindrical kucheman
wetareaBWBck=3778.2+46.704;


VcrucBWBck=Vcruc380;

FBWBck=CalculateconsumptionBWB(wetareaBWBck);
OEWBWBck=CalculateOEWBWB(wetareaBWBck);
DBWBck=CalculateDBWB(wetareaBWBck);

%Standard
wetareaBWBs=3050;
wingareaBWBs=1368.22;

VcrucBWBs=Vcruc380;
```

```
334
335 FBWBs=CalculateconsumptionBWB(wetareaBWBs);
336 OEWBWBs=CalculateOEWBWB(wetareaBWBs);
337 DBWBs=CalculateDBWB(wetareaBWBs);
338 MTOWs=CalculateMTOWBWB(wingareaBWBs);
339 %Ellipsoid
340 wetareaBWBe=3051;
341 wingareaBWBe=1231.76;
342
343 VcrucBWBe=Vcruc380;
344
345 FBWBe=CalculateconsumptionBWB(wetareaBWBe);
346 OEWBWBe=CalculateOEWBWB(wetareaBWBe);
347 DBWBe=CalculateDBWB(wetareaBWBe);
348 MTOWe=CalculateMTOWBWB(wingareaBWBe);
349 %Cylindrical integrated
350 wetareaBWBci=3432.09;
351 wingareaBWBci=1214.3;
352
353 VcrucBWBci=Vcruc380;
354
355 FBWBci=CalculateconsumptionBWB(wetareaBWBci);
356 OEWBWBci=CalculateOEWBWB(wetareaBWBci);
357 DBWBci=CalculateDBWB(wetareaBWBci);
358 MTOWci=CalculateMTOWBWB(wingareaBWBci);
359 %Cylindrical
360 wetareaBWBc=3778.2;
361 wingareaBWBc=1214.3;
362
363 VcrucBWBc=Vcruc380;
364
365 FBWBc=CalculateconsumptionBWB(wetareaBWBc);
366 OEWBWBc=CalculateOEWBWB(wetareaBWBc);
367 DBWBc=CalculateDBWB(wetareaBWBc);
368 MTOWc=CalculateMTOWBWB(wingareaBWBc);
369 %CDBWB=2*DBWB/(rho*V*V*S);
370
371 %StructuralweightBWB= f(wetarea,Structuralweight);
372
373 L=16; %Longitud cilindro (o tanque en si, el parametro de
      profundidad eliptica)
374
375 [Vols,ms,Ths] = Calculatehydroparam(FBWBs,VcrucBWBs,L);
376 [Vole,me,The] = Calculatehydroparam(FBWBe,VcrucBWBe,L);
377 [Volc,mc,Thc] = Calculatehydroparam(FBWBc,VcrucBWBc,L);
378 [Volci,mci,Thci] = Calculatehydroparam(FBWBci,VcrucBWBci,L);
379
380 [Volsk,msk,Thsk] = Calculatehydroparam(FBWBsk,VcrucBWBs,L);
```

```
381 [Volek,mek,Thek] = Calculatehydroparam(FBWBek,VcrucBWBe,L);
382 [Volck,mck,Thck] = Calculatehydroparam(FBWBck,VcrucBWBc,L);
383 [Volcik,mcik,Thcik] = Calculatehydroparam(FBWBcik,VcrucBWBci,L);
384
385 [Vol380,m380,Th380] = Calculatehydroparam(F380,VcrucBWBci,L);
386 %% FUNCION CALCULO ESPECIFICACIONES TANQUE
387 function [V,m,Th] = Calculatehydroparam(F,Vcruc,L)
388     %%Calculate cilindrical hydrogen tank radius.
389     rhofuel=0.812;%kg/l
390     d=15200;%km
391     %Multiplicamos por 4 porque para llevar la misma cantidad de
392     %combustible de hidrogeno que de queroseno se ocupa 4 veces
            mas.
393
394     %Unidades F de kg/s
395
396     %Vcrucero entre 1000 pq esta en m/s y lo queremos en km/s
397
398     FoSVolume=1.2;
399
400     V=4*FoSVolume*F/((rhofuel*1000)*(Vcruc/1000))*d;%en m^3
401     %V=1200; %Volumen necesario. Cuando lo junte con Bada sera: V
            =C*d
402
403     R=1; %Radio cilindro (o la "a" del elipsoide)
404     c=0;
405     Vcont1=0;
406     Vcont01=0;
407     Vcont001=0;
408     Vcont0001=0;
409     Vcont00001=0;
410     Vcont000001=0;
411     Vcont0000001=0;
412     dr=1;
413     while c==0
414         Vcont1=4*pi*((R+1)^3)/3 + pi*L*((R+1)^2);
415         Vcont01=4*pi*((R+0.1)^3)/3 + pi*L*((R+0.1)^2);
416         Vcont001=4*pi*((R+0.01)^3)/3 + pi*L*((R+0.01)^2);
417         Vcont0001=4*pi*((R+0.001)^3)/3 + pi*L*((R+0.001)^2);
418         Vcont00001=4*pi*((R+0.0001)^3)/3 + pi*L*((R+0.0001)^2);
419         Vcont000001=4*pi*((R+0.00001)^3)/3 + pi*L*((R+0.00001)^2);
420         Vcont0000001=4*pi*((R+0.000001)^3)/3 + pi*L*((R+0.000001)
                ^2);
421         if ( V >= Vcont1)
422             dr=1;
423         elseif ( V >= Vcont01)
424             dr=0.1;
425         elseif ( V >= Vcont001)
```

```
426             dr=0.01;
427         elseif ( V >= Vcont0001)
428             dr=0.001;
429         elseif ( V >= Vcont00001)
430             dr=0.0001;
431         elseif ( V >= Vcont000001)
432             dr=0.00001;
433         elseif ( V >= Vcont0000001)
434             dr=0.000001;
435         else
436             c=1;
437         end
438         R=R+dr;
439     end
440
441     % Calculate hydrogen tank thickness
442
443     Sigma=172.4*(10^6); %Material de la NASA segun articulo
            explicado en report
444
445     Pc=145000;%Cryogenic Pressure(Segun articulo NASA) /otro
            articulo dice de 300000 a 600000
446
447     FoS=1.5;%Factor of Safety
448
449     %Thickness
450     T=Pc*R*FoS/(2*Sigma);
451
452     %REAL thickness:
453     F=1;%Factor de cambio de geometria(cambiar de cilindrico a
            elipsoidal por ejemplo)
454     Th=T*F;
455     %Tank material density
456     rhot=2825;
457
458     %%Tank weight
459     m=rhot*(4*pi*((R+Th)^3)/3 + pi*L*((R+Th)^2)-V);
460 end
461
462 %% FUNCION CALCULO FBWB
463 function FBWB = CalculateconsumptionBWB(S)
464 FBWB=-0.00000005*(S^2) + 0.001*S -0.0046;
465 end
466
467 %% FUNCION CALCULO DBWB
468 function DBWB = CalculateDBWB(S)
469 DBWB=-0.0039*(S^2) + 76.932*S - 8689.7;
470 end
```

```
471 %% FUNCION CALCULO OEWBWB
472 function OEWBWB = CalculateOEWBWB(S)
473 OEWBWB=50.473*S + 6317.1;
474 end
475
476 %% FUNCION CALCULO MTOW
477 function MTOWBWB = CalculateMTOWBWB(Swing)
478 MTOWBWB=1645.2*Swing + 19463;
479 end
480 %% FUNCION CALCULO F
481 function [D,Fmean] = Calculateconsumption(model,Vcruc)
482     %READ
483     xml_file = strcat('BADA\',model,'\',model,'.xml');
484     xml = xml2struct(xml_file);
485
486     %Diferent mass;
487     mref_struct = xml.bada40_colon_ACM.PFM.MREF;
488     mref_cell = struct2cell(mref_struct);
489     mref = str2double(mref_cell);
490
491     mmin_struct = xml.bada40_colon_ACM.ALM.DLM.MLW;
492     mmin_cell = struct2cell(mmin_struct);
493     mmin = str2double(mmin_cell);
494
495     mmax_struct = xml.bada40_colon_ACM.ALM.DLM.MTOW;
496     mmax_cell = struct2cell(mmax_struct);
497     mmax = str2double(mmax_cell);
498
499     mmean = (mmax+mmin)/2;
500
501
502     S_struct = xml.bada40_colon_ACM.AFCM.S;
503     S_cell = struct2cell(S_struct);
504     S = str2double(S_cell);
505
506
507 [D1,F1]=calculateconsumwithmas(S,mref,mmin,Vcruc,xml);
508 [D2,F2]=calculateconsumwithmas(S,mref,mmean,Vcruc,xml);
509 [D3,F3]=calculateconsumwithmas(S,mref,mmax,Vcruc,xml);
510
511 Fmean=(F1+F2+F3)/3;
512 D(1)=D1;
513 D(2)=D2;
514 D(3)=D3;
515 D=max(D);
516 end
517 function [D,F] = calculateconsumwithmas(S,mref,m,Vcruc,xml)
518     %General constants
```

```
519     k=1.4;
520     Rair=287.05287;
521     g0=9.80665;
522     bethaT=-0.0065;
523
524     Ttropo=216.65;
525     T0=288.15;
526     theta=Ttropo/T0;
527
528     P0=101325;
529     Ptropo=P0*(theta)^(-g0/(bethaT*Rair));
530     delta=Ptropo/P0;
531
532
533
534     a0=340.29;
535     atropo=sqrt(k*Ttropo*Rair);
536     M=Vcruc/atropo;
537     Wref = mref*g0;
538     %% Calculation of cl
539     Cl=2*m*g0/(delta*P0*k*S*(M^2));
540
541     %% Calculation of cd
542
543     %READ
544     Mmax_struct = xml.bada40_colon_ACM.AFCM.Configuration{1,1}.
            LGUP.DPM_clean.M_max;
545     Mmax_cell = struct2cell(Mmax_struct);
546     Mmax = str2double(Mmax_cell);
547
548     if (M<=Mmax)
549         Cd = calculatecdbelow(M,Cl,xml);
550     else
551         CdMmax = calculatecdbelow(Mmax,Cl,xml);
552         CdMmax_ = calculatecdbelow(M-0.01,Cl,xml);
553
554         Cd = CdMmax_ + ((((M+0.01-Mmax)/0.01)^(3/2))*(CdMmax -
                CdMmax_));
555     end
556
557     %% Calculation of D
558
559     D = delta * P0 * k * S * (M^2) * Cd/2;
560
561     %% Calculation of CT (coef of thrust)
562
563     %Note that T=D
564     Ct = D/(Wref*delta);
```

```
565
566     %% Calculation of Cf (fuel coeficient)
567     %READ
568     CF = xml.bada40_colon_ACM.PFM.TFM.LIDL.CF;
569     fi_struct = [CF.fi{1};
570                  CF.fi{2};
571                  CF.fi{3};
572                  CF.fi{4};
573                  CF.fi{5};
574                  CF.fi{6};
575                  CF.fi{7};
576                  CF.fi{8};
577                  CF.fi{9};
578                  ];
579     fi_cell = struct2cell(fi_struct);
580     fi = str2double(fi_cell);
581
582     fi1=fi(1);
583     fi2=fi(2);
584     fi3=fi(3);
585     fi4=fi(4);
586     fi5=fi(5);
587     fi6=fi(6);
588     fi7=fi(7);
589     fi8=fi(8);
590     fi9=fi(9);
591
592     fisum=fi1 + fi2*delta + fi3*(delta^2) + (fi4 + fi5*delta +
          fi6*(delta^2))*M + (fi7 + fi8*delta + fi9*(delta^2))*(M^2)
          ;
593
594     Cfidle= (fisum)/(delta * (theta^(1/2)));
595
596     %READ
597     CF2 = xml.bada40_colon_ACM.PFM.TFM.CF;
598     f_struct = [CF2.f{1};
599                 CF2.f{2};
600                 CF2.f{3};
601                 CF2.f{4};
602                 CF2.f{5};
603                 CF2.f{6};
604                 CF2.f{7};
605                 CF2.f{8};
606                 CF2.f{9};
607                 CF2.f{10};
608                 CF2.f{11};
609                 CF2.f{12};
610                 CF2.f{13};
```

```
                CF2.f{14};
                CF2.f{15};
                CF2.f{16};
                CF2.f{17};
                CF2.f{18};
                CF2.f{19};
                CF2.f{20};
                CF2.f{21};
                CF2.f{22};
                CF2.f{23};
                CF2.f{24};
                CF2.f{25};
                ];
    f_cell = struct2cell(f_struct);
    f = str2double(f_cell);

    % f_struct = xml.bada40_colon_ACM.PFM.TFM.CF;
    % f_cell = struct2cell(f_struct);
    % f = str2double(f_cell);

    f1=f(1);
    f2=f(2);
    f3=f(3);
    f4=f(4);
    f5=f(5);
    f6=f(6);
    f7=f(7);
    f8=f(8);
    f9=f(9);
    f10=f(10);
    f11=f(11);
    f12=f(12);
    f13=f(13);
    f14=f(14);
    f15=f(15);
    f16=f(16);
    f17=f(17);
    f18=f(18);
    f19=f(19);
    f20=f(20);
    f21=f(21);
    f22=f(22);
    f23=f(23);
    f24=f(24);
    f25=f(25);

    Cf15=f1 + f2*Ct + f3*(Ct^2) + f4*(Ct^3) + f5*(Ct^4);
    Cf510=f6 + f7*Ct + f8*(Ct^2) + f9*(Ct^3) + f10*(Ct^4);
```

```
659       Cf1015=f11 + f12*Ct + f13*(Ct^2) + f14*(Ct^3) + f15*(Ct^4);
660       Cf1520=f16 + f17*Ct + f18*(Ct^2) + f19*(Ct^3) + f20*(Ct^4);
661       Cf2025=f21 + f22*Ct + f23*(Ct^2) + f24*(Ct^3) + f25*(Ct^4);
662
663       Cfgen= Cf15 + Cf510*M + Cf1015*(M^2) + Cf1520*(M^3) + Cf2025
              *(M^4);
664
665       Cf=max(Cfidle,Cfgen);
666
667       %% Calculation of F (fuel consumption)
668
669       %READ
670
671       LHV_struct = xml.bada40_colon_ACM.PFM.LHV;
672       LHV_cell = struct2cell(LHV_struct);
673       LHV = str2double(LHV_cell);
674
675
676       F= delta * Wref * a0 * (theta^(1/2)) * Cf/LHV;
677
678   end
679   %% FUNCTIONS
680   function [Cd] = calculatecdbelow(M,Cl,xml)
681       %READ
682       DPM_clean = xml.bada40_colon_ACM.AFCM.Configuration{1,1}.LGUP
              .DPM_clean;
683       d_struct = [DPM_clean.CD_clean.d{1};
684                   DPM_clean.CD_clean.d{2};
685                   DPM_clean.CD_clean.d{3};
686                   DPM_clean.CD_clean.d{4};
687                   DPM_clean.CD_clean.d{5};
688                   DPM_clean.CD_clean.d{6};
689                   DPM_clean.CD_clean.d{7};
690                   DPM_clean.CD_clean.d{8};
691                   DPM_clean.CD_clean.d{9};
692                   DPM_clean.CD_clean.d{10};
693                   DPM_clean.CD_clean.d{11};
694                   DPM_clean.CD_clean.d{12};
695                   DPM_clean.CD_clean.d{13};
696                   DPM_clean.CD_clean.d{14};
697                   DPM_clean.CD_clean.d{15}
698               ];
699       d_cell = struct2cell(d_struct);
700       d = str2double(d_cell);
701       d1=d(1);
702       d2=d(2);
703       d3=d(3);
704       d4=d(4);
```

```
705       d5=d(5);
706       d6=d(6);
707       d7=d(7);
708       d8=d(8);
709       d9=d(9);
710       d10=d(10);
711       d11=d(11);
712       d12=d(12);
713       d13=d(13);
714       d14=d(14);
715       d15=d(15);
716
717       scalar_struct = xml.bada40_colon_ACM.AFCM.Configuration{1,1}.
              LGUP.DPM_clean.scalar;
718       scalar_cell = struct2cell(scalar_struct);
719       scalar = str2double(scalar_cell);
720
721
722       C0= d1 + d2/((1-M^2)^(1/2)) + d3/((1-M^2)^(1)) + d4/(1-M^2)
              ^(3/2) + d5/(1-M^2)^(2);
723       C2= d6 + d7/((1-M^2)^(3/2)) + d8/((1-M^2)^(3)) + d9/(1-M^2)
              ^(9/2) + d10/(1-M^2)^(6);
724       C6= d11 + d12/((1-M^2)^(7)) + d13/((1-M^2)^(15/2)) + d14/(1-M
              ^2)^(8) + d15/(1-M^2)^(17/2);
725
726       Cd= scalar * (C0 + C2*(Cl^2) + C6*(Cl^6));
727   end
728
729   %% give me structural weightfunction
730   function [ OEW ] = givemeW( model )
731       xml_file = strcat('BADA\',model,'\',model,'.xml');
732       xml = xml2struct(xml_file);
733
734       %BADA STRUCTURAL WEIGHT
735       OEW_struct = xml.bada40_colon_ACM.ALM.DLM.OEW;
736       OEW_cell = struct2cell(OEW_struct);
737       OEW = str2double(OEW_cell);
738   end
739   %% xml2structfunction
740
741   function [ s ] = xml2struct( file )
742   %Convert xml file into a MATLAB structure
743   % [ s ] = xml2struct( file )
744   %
745   % A file containing:
746   % <XMLname attrib1="Some value">
747   %   <Element>Some text</Element>
748   %   <DifferentElement attrib2="2">Some more text</Element>
```

```
749 %   <DifferentElement attrib3="2" attrib4="1">Even more text</
        DifferentElement>
750 % </XMLname>
751 %
752 % Will produce:
753 % s.XMLname.Attributes.attrib1 = "Some value";
754 % s.XMLname.Element.Text = "Some text";
755 % s.XMLname.DifferentElement{1}.Attributes.attrib2 = "2";
756 % s.XMLname.DifferentElement{1}.Text = "Some more text";
757 % s.XMLname.DifferentElement{2}.Attributes.attrib3 = "2";
758 % s.XMLname.DifferentElement{2}.Attributes.attrib4 = "1";
759 % s.XMLname.DifferentElement{2}.Text = "Even more text";
760 %
761 % Please note that the following characters are substituted
762 % '-' by '_dash_', ':' by '_colon_' and '.' by '_dot_'
763 %
764 % Written by W. Falkena, ASTI, TUDelft, 21-08-2010
765 % Attribute parsing speed increased by 40% by A. Wanner,
        14-6-2011
766 % Added CDATA support by I. Smirnov, 20-3-2012
767 %
768 % Modified by X. Mo, University of Wisconsin, 12-5-2012
769
770     if (nargin < 1)
771         clc;
772         help xml2struct
773         return
774     end
775
776     if isa(file, 'org.apache.xerces.dom.DeferredDocumentImpl') ||
            isa(file, 'org.apache.xerces.dom.DeferredElementImpl')
777         % input is a java xml object
778         xDoc = file;
779     else
780         %check for existance
781         if (exist(file,'file') == 0)
782             %Perhaps the xml extension was omitted from the file
                    name. Add the
783             %extension and try again.
784             if (isempty(strfind(file,'.xml')))
785                 file = [file '.xml'];
786             end
787
788             if (exist(file,'file') == 0)
789                 error(['The file ' file ' could not be found']);
790             end
791         end
792         %read the xml file
```

```
793             xDoc = xmlread(file);
794         end
795 
796         %parse xDoc into a MATLAB structure
797         s = parseChildNodes(xDoc);
798 
799     end
800 
801     % ------ Subfunction parseChildNodes ------
802     function [children,ptext,textflag] = parseChildNodes(theNode)
803         % Recurse over node children.
804         children = struct;
805         ptext = struct; textflag = 'Text';
806         if hasChildNodes(theNode)
807             childNodes = getChildNodes(theNode);
808             numChildNodes = getLength(childNodes);
809 
810             for count = 1:numChildNodes
811                 theChild = item(childNodes,count-1);
812                 [text,name,attr,childs,textflag] = getNodeData(
                        theChild);
813 
814                 if (~strcmp(name,'#text') && ~strcmp(name,'#comment')
                         && ~strcmp(name,'#cdata_dash_section'))
815                     %XML allows the same elements to be defined
                            multiple times,
816                     %put each in a different cell
817                     if (isfield(children,name))
818                         if (~iscell(children.(name)))
819                             %put existsing element into cell format
820                             children.(name) = {children.(name)};
821                         end
822                         index = length(children.(name))+1;
823                         %add new element
824                         children.(name){index} = childs;
825                         if(~isempty(fieldnames(text)))
826                             children.(name){index} = text;
827                         end
828                         if(~isempty(attr))
829                             children.(name){index}.('Attributes') =
                                    attr;
830                         end
831                     else
832                         %add previously unknown (new) element to the
                                structure
833                         children.(name) = childs;
834                         if(~isempty(text) && ~isempty(fieldnames(text
                                )))
```

```
835                         children.(name) = text;
836                     end
837                     if(~isempty(attr))
838                         children.(name).('Attributes') = attr;
839                     end
840                 end
841             else
842                 ptextflag = 'Text';
843                 if (strcmp(name, '#cdata_dash_section'))
844                     ptextflag = 'CDATA';
845                 elseif (strcmp(name, '#comment'))
846                     ptextflag = 'Comment';
847                 end
848 
849                 %this is the text in an element (i.e., the
                        parentNode)
850                 if (~isempty(regexprep(text.(textflag),'[\s]*',''
                    )))
851                     if (~isfield(ptext,ptextflag) || isempty(
                        ptext.(ptextflag)))
852                         ptext.(ptextflag) = text.(textflag);
853                     else
854                         %what to do when element data is as
                            follows:
855                         %<element>Text <!--Comment--> More text</
                            element>
856 
857                         %put the text in different cells:
858                         % if (~iscell(ptext)) ptext = {ptext};
                            end
859                         % ptext{length(ptext)+1} = text;
860 
861                         %just append the text
862                         ptext.(ptextflag) = [ptext.(ptextflag)
                            text.(textflag)];
863                     end
864                 end
865             end
866 
867         end
868     end
869 end
870 
871 %------ Subfunction getNodeData ------
872 function [text,name,attr,childs,textflag] = getNodeData(theNode)
873     % Create structure of node info.
874 
875     %make sure name is allowed as structure name
```

```
876       name = toCharArray(getNodeName(theNode))';
877       name = strrep(name, '-', '_dash_');
878       name = strrep(name, ':', '_colon_');
879       name = strrep(name, '.', '_dot_');
880
881       attr = parseAttributes(theNode);
882       if (isempty(fieldnames(attr)))
883           attr = [];
884       end
885
886       %parse child nodes
887       [childs,text,textflag] = parseChildNodes(theNode);
888
889       if (isempty(fieldnames(childs)) && isempty(fieldnames(text)))
890           %get the data of any childless nodes
891           % faster than if any(strcmp(methods(theNode), 'getData'))
892           % no need to try-catch (?)
893           % faster than text = char(getData(theNode));
894           text.(textflag) = toCharArray(getTextContent(theNode))';
895       end
896
897   end
898
899   %------ Subfunction parseAttributes ------
900   function attributes = parseAttributes(theNode)
901       % Create attributes structure.
902
903       attributes = struct;
904       if hasAttributes(theNode)
905          theAttributes = getAttributes(theNode);
906          numAttributes = getLength(theAttributes);
907
908          for count = 1:numAttributes
909               %attrib = item(theAttributes,count-1);
910               %attr_name = regexprep(char(getName(attrib))
                     ,'[-:.]','_');
911               %attributes.(attr_name) = char(getValue(attrib));
912
913               %Suggestion of Adrian Wanner
914               str = toCharArray(toString(item(theAttributes,count
                     -1)))';
915               k = strfind(str,'=');
916               attr_name = str(1:(k(1)-1));
917               attr_name = strrep(attr_name, '-', '_dash_');
918               attr_name = strrep(attr_name, ':', '_colon_');
919               attr_name = strrep(attr_name, '.', '_dot_');
920               attributes.(attr_name) = str((k(1)+2):(end-1));
921          end
```

```
922         end
923     end
```

APPENDIX D. POST-PROCESSING

The post-processing analysis allow us to understand and validate the results of a simulation and found unexpected effects. Thus, a set of pressure and velocity contours in different planes have been included in this section. The pressure differences have been computed with respect to calm atmosphere pressure. For greater pressure, lower fluid velocity (eq Bernoulli) something that can be observed in the images of the post processing (figure D.1 VS D.11 for example), so practically, everything mentioned about pressure can also be concluded with speed contours.

There is only difference between BWB_e and BWB_c contours in the planes that includes the blunt body. In the rest of the contours, a similar behavior can be observed, because the geometry of the aircraft in those projections is the same for both models (figures D.5, D.6, D.7 and D.8). The BWB_e is much more similar to what should be seen in the simulation of an alar profile, and thus, as expected, it will generate more lift and less drag (figure D.1/D.3/D.9 VS D.2/D.4/D.10). The introduction of a blunt body increases the pressure in that area and, hence, decreases the velocity of the fluid. The nose of the hydrogen tank behaves like the nose of the aircraft (figures D.5 and D.9).

The large detachment observed in the rear of the aircraft (figures D.15 and D.16) in the plane of symmetry can be produced by the vertical stabilizer, since in the wing area a less affection can be observed (figure D.20) and, nevertheless, in the hydrogen tank a large detachment can be observed, due to its blunt shape (figure D.19).

As can be observed, there is a large detachment in the walls of the control volume (figure D.18), which should not appear on a flight (although appears in the wind tunnel). This is because the non-slip condition has been defined. To verify that this setting does not affect the results, a simulation with a slip condition was generated, thus obtaining the same result in both cases.

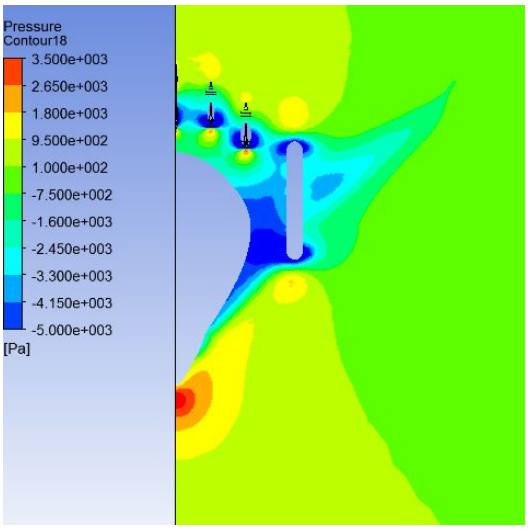

Figure D.1: Pressure contours of BWB_{ci} in plane y=0

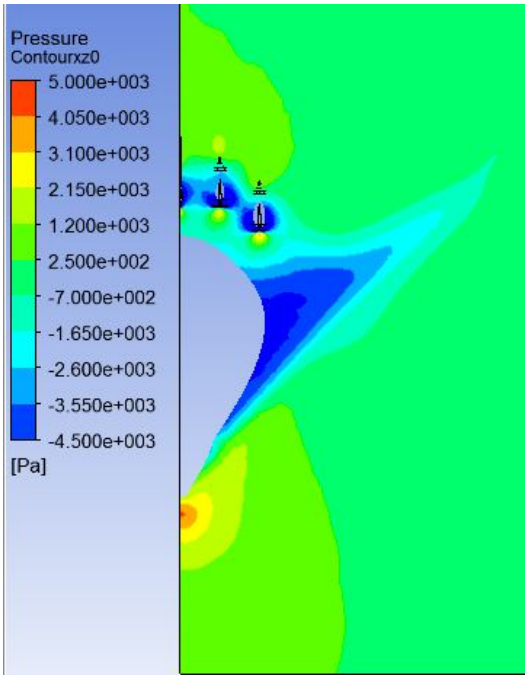

Figure D.2: Pressure contours of BWB_e V2 in plane y=0

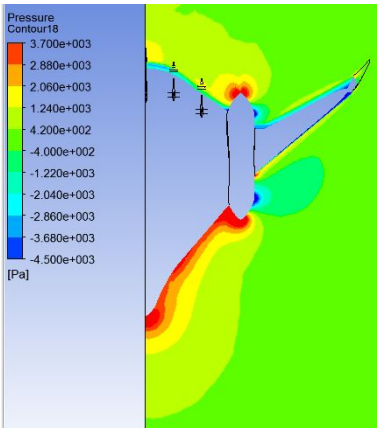

Figure D.3: Pressure contours of BWB_{ci} in plane y= -2 m

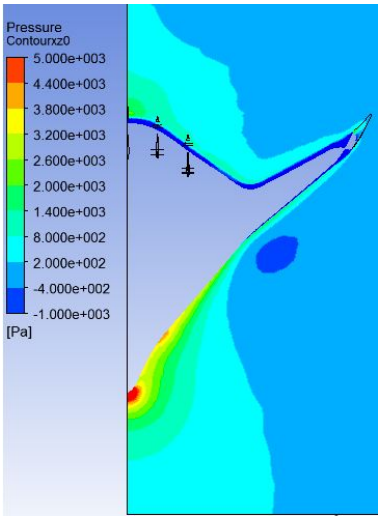

Figure D.4: Pressure contours of BWB_e V2 in plane y= -2 m

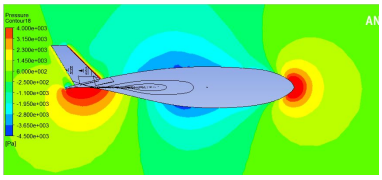

Figure D.5: Pressure contours of BWB_{ci} in symmetry plane

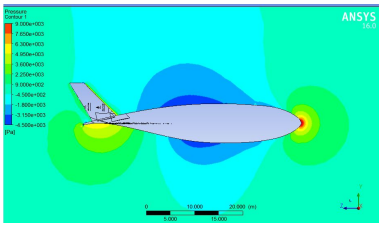

Figure D.6: Pressure contours of BWB_e V2 in symmetry plane

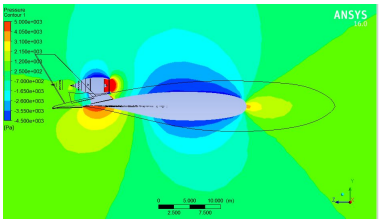

Figure D.7: Pressure contours of BWB_{ci} in plane x=10

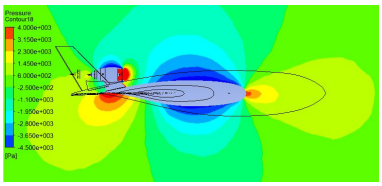

Figure D.8: Pressure contours of BWB_e V2 in plane x=10

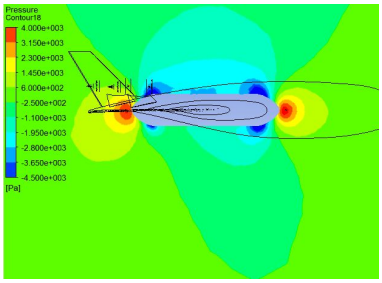

Figure D.9: Pressure contours of BWB_{ci} in plane x=18

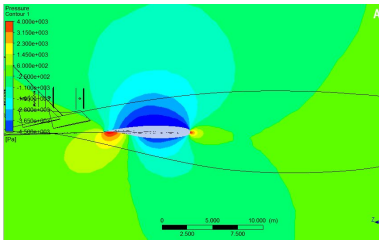

Figure D.10: Pressure contours of BWB_e V2 in plane x=20

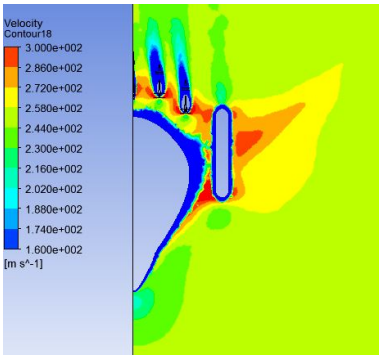

Figure D.11: Velocity contours of BWB_{ci} in plane y=0

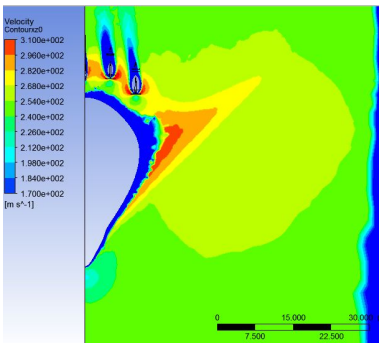

Figure D.12: Velocity contours of BWB_e V2 in plane y=0

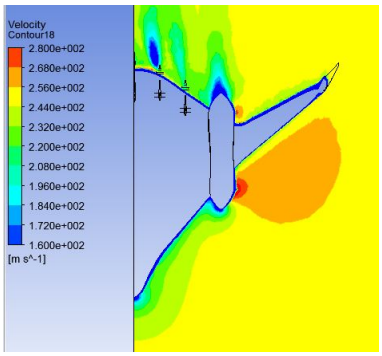

Figure D.13: Velocity contours of BWB_{ci} in plane y= -2 m

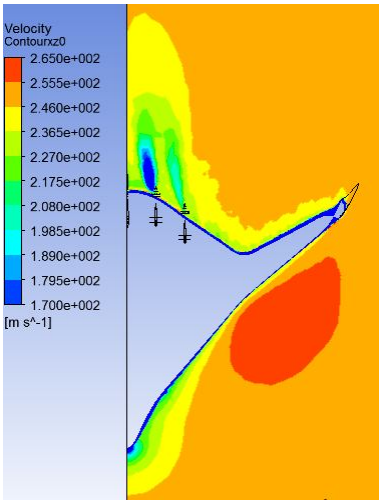

Figure D.14: Velocity contours of BWB_e V2 in plane y= -2 m

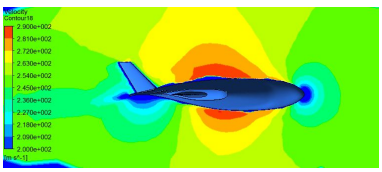

Figure D.15: Velocity contours of BWB_{ci} in symmetry plane

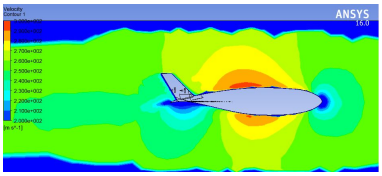

Figure D.16: Velocity contours of BWB_e V2 in symmetry plane

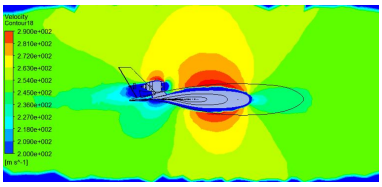

Figure D.17: Velocity contours of BWB_{ci} in plane x=10

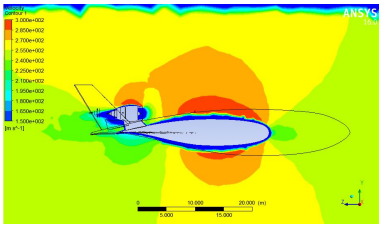

Figure D.18: Velocity contours of BWB_e V2 in plane x=10

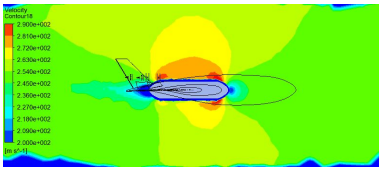

Figure D.19: Velocity contours of BWB_{ci} in plane x=18

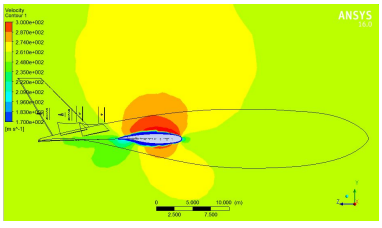

Figure D.20: Velocity contours of BWB_{ci} in plane x=20